國立臺灣大學電機資訊學院生醫電子與資訊學研究所

碩士論文

Graduate Institute of Biomedical Electronics and Bioinformatics
College of Electrical Engineering and Computer Science
National Taiwan University

Master's Thesis

利用雙閘極敏感場效應電晶體結合離子選擇膜及微流道進行水質六價鉻離子濃度檢測

Ion Selective Membrane with Dual-Gate Ion-Sensitive Field-Effect Transistor (ISFET) Integrating the Microfluidic Channel for Chromium(VI) Ion Detection in Water

劉子瑜

Tzu-Yu Liu

指導教授：黃念祖 博士

Advisor: Nien-Tsu Huang, Ph.D.

中華民國 113 年 5 月

May 2024

doi:10.6342/NTU202401040

國立臺灣大學碩士學位論文
口試委員會審定書
MASTER'S THESIS ACCEPTANCE CERTIFICATE
NATIONAL TAIWAN UNIVERSITY

利用雙閘極敏感場效應電晶體結合離子選擇膜及微流道進行水質六價鉻離子濃度檢測

Ion Selective Membrane with Dual-Gate Ion-Sensitive Field-Effect Transistor (ISFET) Integrating the Microfluidic Channel for Chromium(VI) Ion Detection in Water

本論文係 劉子瑜 R10945042 在國立臺灣大學電機資訊學院生醫電子與資訊學研究所完成之碩士學位論文，於民國 113 年 3 月 15 日承下列考試委員審查通過及口試及格，特此證明。

The undersigned, appointed by the Graduate Institute of Biomedical Electronics and Bioinformatics, National Taiwan University on 15, March 2024 have examined a Master's thesis entitled above presented by Tzu-Yu, Liu R10945042 candidate and hereby certify that it is worthy of acceptance.

口試委員 Oral examination committee:

黃念祖 _____ 盧彥文 _____ _____

（指導教授 Advisor）

林致廷 _____ 曾璟瑋 _____ _____

系主任/所長 Director: 林致廷 _____

doi:10.6342/NTU202401040

誌謝

這篇論文乘載著我這三年的鍛鍊、思考、苦痛與成長。首先我要感謝我自己，謝謝你一直努力到現在而沒有放棄。你肯定覺得現在的階段還不足以被稱讚，所以就由我在這裡頌揚並感激你所做的一切掙扎與選擇。你跨過了自我貶低和冒名頂替的階段，雖仍被消磨著卻還是振作了起來，每一天你都在漸漸成長跟學習新技能、新思維，了解交涉的重要性，知道抓對方向比埋頭苦幹更重要。你也開始學會自我健康管理，明白腦袋首先是肌肉和身體的奴隸。你開始試著去喜歡自己的優點並了解怎麼樣的工作環境、效率、節奏會讓自己感到開心並從中獲得成就感。最重要的是，你還沒有停止去嘗試讓自己更喜歡你的人生，而這也是我最喜歡你的地方。你肯定事後會覺得很羞恥，但是，謝謝你所做的一切，謝謝你。

再來要謝謝我爸媽，謝謝他們願意讓我啃老到 27 歲，真是一個令人尷尬的數字。但他們從來沒對我的生活或人生選擇指手畫腳過，只是靜靜地聽我說，然後靜靜地支持我，我在長大後才明白這有多難能可貴。在這段日子裡，LOBA 過世了，外公也過世了，我不確定他們是否其實也有自己的心坎要過，畢竟他們也不是什麼愛分享心事給孩子的人。我也不確定自己有沒有達到他們心中的期待，但我想這也不是他們生下我的理由，我首先滿足我對自己的期待，就好了。

再來是聽說在誌謝裡提到的話就會分手的女朋友。這幾年我也漸漸變成一個難搞的人，還好這人尚能忍受。很常被問為甚麼能夠在一起那麼久，是不是有什麼相處小秘訣，我覺得其實就只是我們彼此都足夠尊重對方的人格和興趣而已，還有就是夠幸運。2023 年初一起去了日本，至今仍是我人生中最快樂的出國回憶。基本上都是靠著和你相處的快樂心情和美好回憶去面對挫折與苦難的。我自認人生歐了兩次，一次是生在我家，一次是遇到你。謝謝你。

再來終於輪到實驗室成員。首先是黃念祖老師，我真的很感謝老師在我碩一狀況不佳、研究沒上軌道時，既沒有過度催促，也不曾降低門檻，就只是每週要求我想清楚下一步、踏出下一步、規劃好下一步，維持著研究節奏而已。這三年來，一直堅持、打磨、改進我的研究，某種程度上可以說比我自己還更相信我的研究可以更完整、更有趣。能夠遇到這樣的導師，我想是十分難能可貴的。

doi:10.6342/NTU202401040

接著是快樂夥伴的王鈞、明儒、彥安。為了感謝你們而將誌謝寫到兩頁，我覺得沒什麼問題，畢竟這可是我的論文。長年待在你們身邊，我也從你們身上學到了很多。彥安的做事效率真的是我看過一等一的快速又確實，每週跟你一起個咪搞得我壓力很大，為了不被你甩在後面我也是卯足了勁做研究，基本上你功不可沒。王鈞就是唯一的準時畢業之神，這兩年來看著你又當邱比特，又當雜事處理大師，還能把自己研究搞定。你花在研究上的時間跟心力是如此扎實，除了尊敬跟佩服也是無話可說。希望你能找到屬於自己的邱比特。明儒從非相關科系轉過來，還能夠完成此等研究，此等努力家心態我想應該是從楓之谷肝出來的。你的流道設計最為複雜，還能搞定那麼多的參數並完成既定的目標，基本上我只能說不錯，還得是你。

再來是曉汶跟家靖，雖然我也不知道他們會不會看到我的論文。謝謝你們給了我很多初期做實驗的點子跟初入實驗室的教導。還有前博班學長大涵，給了我非常多切入問題的角度和分析整體研究的思維和方向，只能說不愧是大學長，有夠罩。以及 Labridge 博班同學淮原，在我猶豫該如何呈現研究成果時，給了我很多方向與建議，不愧是經歷過碩班生活的男人。再來是天天都在笑的 VT 好朋友啟耀，你廚的程度是真的誇張，基本上是一台 VSPO 監視器。還有被我拐進來的宣融，你能在兩年內完成那麼多事情並成功出國是真的很厲害，你的做事效率也跟彥安一樣誇張，我每次個咪真的壓力很大。然後是同齡的冠均，能夠聊各式各樣的話題、人生方向與心路歷程。能夠有你在實驗室給予建議是真的很安心也很有幫助。最後是同為 EE 出身的彥程，還好有你在，不然大家對 EE 的評價可能要降低，基本上是從頭秀到尾。在京都之旅能夠和你們一起真的很快樂，謝謝你們充實了我這三年的人生。

當初的我順著身邊人的趨勢來唸碩士，這三年生活給了我很多震撼教育，但回頭一看都是給予當時的我最適合的挑戰。現在的我可以很驕傲地宣稱這趟旅程不虛此行。我努力過了，也成功了。謝謝你們，謝謝我。

doi:10.6342/NTU202401040

中文摘要

水質重金屬離子濃度檢測為檢驗水質品質的一大指標。但傳統量測技術往往需要專業技術人員於實驗室操作精密儀器才能得到檢驗結果，而樣品運送途中也可能對樣本產生影響，造成量測誤差。為解決傳統技術問題，我們開發出一種整合雙閘極離子敏感場效電晶體(Dual-gate ion-selective field-effect transistor, DG-ISFET)的微流道裝置進行水質重金屬檢測。本裝置使用離子選擇膜(Ion selective membrane, ISM)以捕捉特定離子，並透過 DG-ISFET 量測捕捉行為所產生的訊號差異，進而確認離子濃度。為驗證上述技術，我們首先使用已知重金屬離子濃度的標準液以最佳化離子選擇膜的體積/表面積比，達到最大的捕捉效率，接著進行 DG-ISFET 結合 ISM 的標準液離子濃度測試，並以相關理論說明 ISM 與重金屬離子的捕捉反應是如何被 DG-ISFET 偵測並記錄。最終我們利用壓力幫浦系統自動注入水圳廢水到流道晶片中進行六價鉻離子捕捉與濃度檢測。此實驗應證了該晶片可在機台最大時長區間持續偵測訊號，並同時含有優異的靈敏度與選擇性。上述的研究結果表明此可攜式水質檢測晶片可用於即時且連續性的自動化水質重金屬離子檢測，並能透過訊號差動量測完全排除環境雜訊，有望在未來將其應用在家用定點水質重金屬檢測、探勘水質重金屬檢測或是搭載於無人機的遠端檢測環境中。

關鍵字：微流體系統、離子選擇膜、離子敏感場效電晶體、六價鉻、重金屬

doi:10.6342/NTU202401040

ABSTRACT

Testing water for heavy metal ions is vital for assessing its quality. However, traditional methods require skilled technicians and complex lab equipment, posing logistical challenges. To address the above problems, we developed a microfluidic device with a Dual-gate Ion-Selective Field-Effect Transistor (ISFET) for heavy metal ion detection. Using an Ion-Selective Membrane (ISM), our device captures target ions and measures the signal difference via ISFET to determine ion concentration. We optimized ISM thickness and concentration of buffer solution using known ion standard solutions to validate our method, achieving maximum capture efficiency. We then evaluated sensing performance against standard ion solutions, elucidating the capture response mechanism. Finally, we tested the device used in ditch wastewater for chromium(VI) ion detection, demonstrating its sensitivity and selectivity. Our findings confirm the device's real-time water quality monitoring potential, with noise reduction capabilities for various applications, including household use and environmental monitoring.

Keywords: Microfluidic channel, ion-selective membrane, ISFET, Chromium(VI), heavy metal ions.

doi:10.6342/NTU202401040

CONTENTS

doi:10.6342/NTU202401040

doi:10.6342/NTU202401040

doi:10.6342/NTU202401040

LIST OF FIGURES

doi:10.6342/NTU202401040

doi:10.6342/NTU202401040

doi:10.6342/NTU202401040

doi:10.6342/NTU202401040

LIST OF TABLES

doi:10.6342/NTU202401040

Chapter 1 Introduction

1.1 Research background

Water is the fundamental necessity in human life. Due to the ongoing pollution of freshwater and the excessive utilization of this precious resource amid rapid urbanization and industrial growth, nearly 40% of the global population is grappling with freshwater inadequacy. Consequently, water pollution emerges as the most pressing challenge that humanity must confront. Wastewater discharged from industrial and daily activities may carry pollutants. Among them, heavy metal ions pose a particularly severe threat. They are toxic and carcinogenic substances that resist decomposition, persisting in the ecosystem for extended periods. Given their increased usage in contemporary society, the potential harm to the human body has markedly escalated [1].

Heavy metals are ubiquitously present in the Lithosphere. The primary culprits behind the pollution of these substances are the extraction, industrial production, utilization, agricultural practices, household applications, and medical uses of heavy metals and their compounds. Furthermore, the corrosion of metals, soil erosion by metal ions, leaching, deposition, re-suspension, and evaporation from water sources to soil and groundwater are significant contributors to the pollution. Natural phenomena, such as weather patterns and volcanic activity, also play a substantial role in the prevalence of heavy metal pollution. Figure 1-1 shows several common heavy metal ions and their sources of environmental contamination.

Arsenic (As), Cadmium (Cd), Copper (Cu), Iron (Fe), Mercury (Hg), Lead (Pb), and Chromium (Cr), among other heavy metals, are considered highly hazardous. These metals readily form sulfur, nitrogen, and oxygen complexes in biological and chemical materials. Consequently, they have the potential to alter the structure of proteins, inhibit

doi:10.6342/NTU202401040

enzymes, and disrupt molecule bonds. As a result, the complex forms of these heavy metals may exhibit carcinogenic effects and impact various physiological systems. It is noteworthy, however, that the human body requires trace amounts of these metals to sustain metabolic processes. Therefore, the World Health Organization (WHO) has established standard concentration limits for these metals in wastewater. The concentration of metal ions below these specified limits is considered safe for consumption.

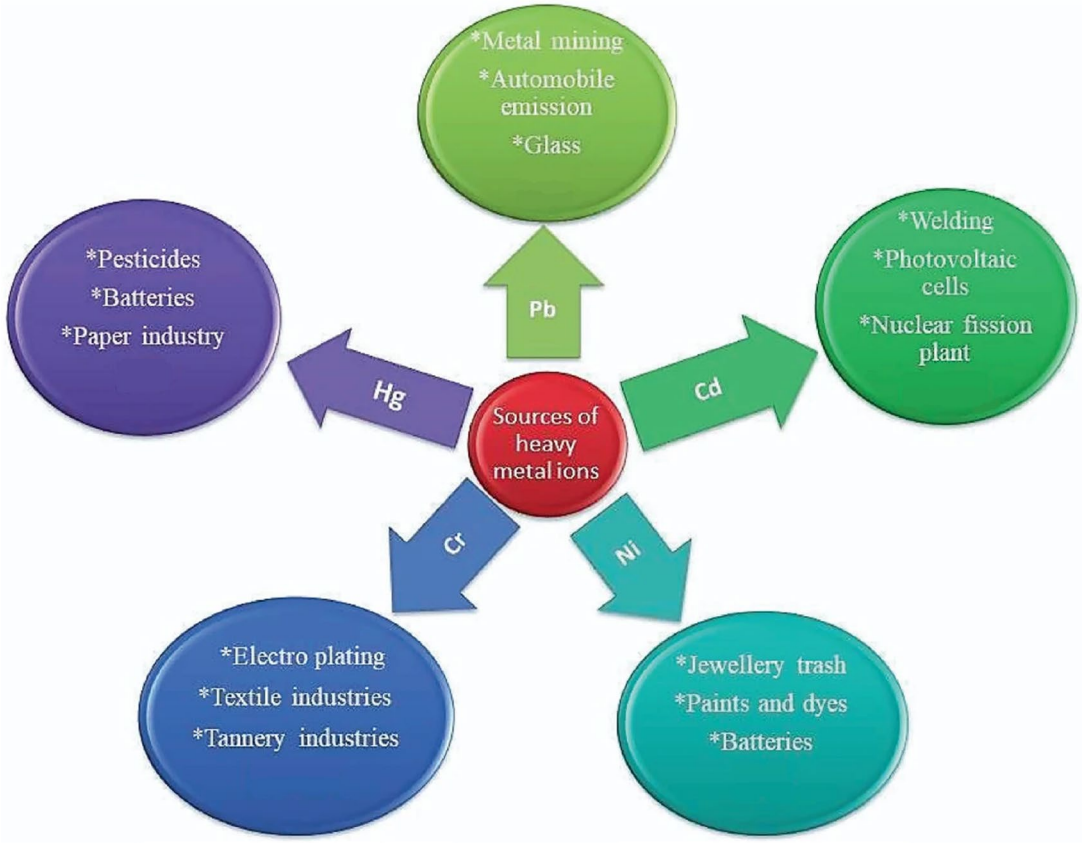

Figure 1-1 Heavy metal ions and their sources in environment contamination [2].

Among all heavy metal ions detections, chromium(VI) (Cr(VI)) has its unique difficulty due to its complex ionic form and its similarity with chromium(III) (Cr(III)), which has relatively low toxicity to Cr(VI). There is an urgent need for precise, reliable, cheap, and expeditious technology for on-site detection of Cr(VI) falling below international standard guideline values.

doi:10.6342/NTU202401040

1.2 Properties of Cr(VI)

Chromium is present in trace amounts in soil, rocks, and various life forms, its atomic weight is 51.9. Chromium could form various salts, with sodium and potassium being the predominant types. Cr(III) and Cr(VI) represent stable forms within chromium ions. Cr(III) occurs in various environments, exhibiting non-toxic properties and providing nutritional benefits to humans. On the other hand, Cr(VI), primarily in the form of chromate and dichromate, is utilized in industries such as dyeing, pigment production, and plating. It is a primary contributor to occupational and environmental contamination. The diverse forms of Cr(VI) are influenced by the pH of the solutions (Figure 1-2). Specifically, at a pH < 1, it exists as H_2CrO_4; at 2 < pH < 4, both dichromate ($Cr_2O_7^{2-}$) and $HCrO_4^-$ coexist; in the pH range of 4 < pH < 6, both dichromate and chromate (CrO_4^{2-}) are present, with chromate becoming dominant below pH < 6.5 (Figure 1-2).

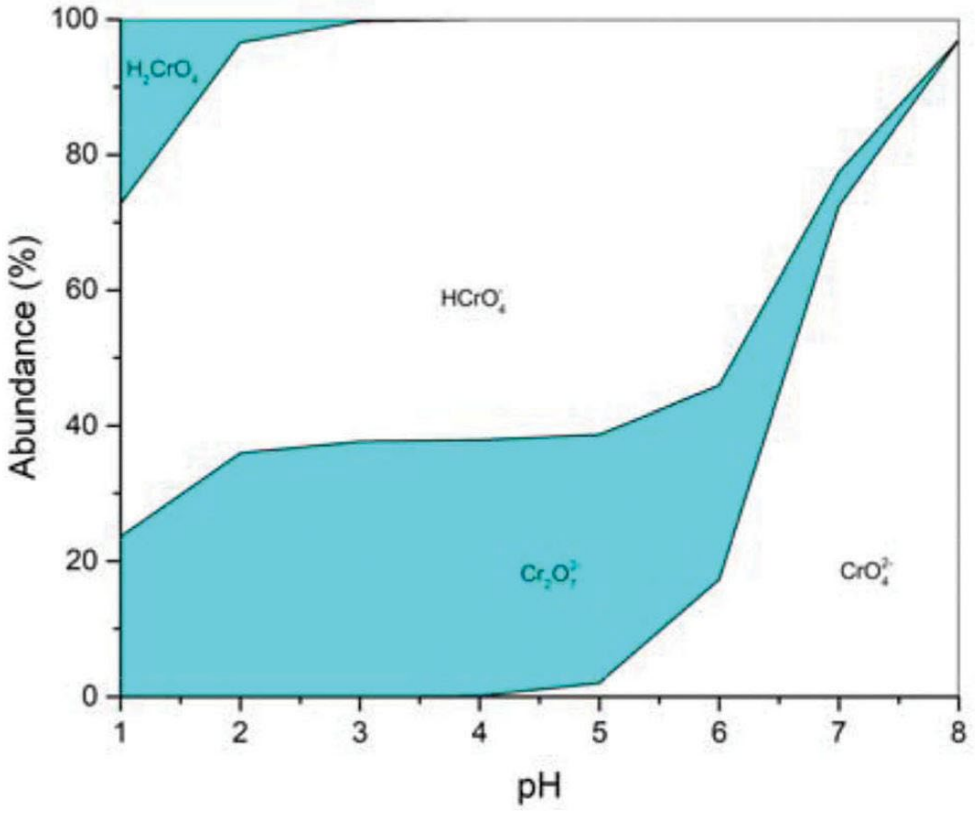

Figure 1-2 The distribution of different Cr(VI) forms in water [3].

doi:10.6342/NTU202401040

1.3 Applications of Cr(VI)

Cr(VI) finds widespread application in numerous industrial processes. Its low solubility in water contributes to its various compounds' distinct and vibrant colors, including yellow lead chromate, brick-red silver chromate, and orange potassium chromate. Due to these unique color properties, Cr(VI) is extensively used in the dye and pigment industry. Moreover, given its elevated hardness, high melting point, and anti-corrosion characteristics, Cr(VI) is employed in diverse applications such as plating, wood preservation, the steel industry, and as an anti-rust additive.

1.4 Toxicity of Cr(VI)

Cr(VI) is recognized as a significant environmental pollutant, with its toxicity attributed to its highly soluble oxidation state. In contrast, Cr(III) is relatively non-toxic, owing to its tendency to form insoluble hydroxides, resulting in reduced leakage into the ecosystem. However, prolonged exposure to high Cr(III) concentrations remains harmful. The toxicity of Cr(VI) is notably elevated, about 500 times higher than Cr(III). Cr(VI), commonly released in manufacturing industries, could infiltrate the soil and contaminate groundwater. Natural Cr(VI) concentrations are minimal, with most existing in a reduced state. Oceanic levels are approximately 0.1-0.5 μg/L, clean surface water ranges from 0.3-0.6 μg/L, increasing to 5-50 μg/L in polluted water and exceeding 200 μg/L in highly contaminated water. The U.S. Environmental Protection Agency has established a crop standard of 100 μg/L for total chromium, with a drinking water standard of 0.1 μg/L, encompassing all chromium forms, including Cr(VI).

Biologically, Cr(VI) could quickly enter the human body through direct pathways, such as mucosal contact, resulting in skin and nasal cavity ulceration, organ function damage, and potentially death. Prolonged exposure to Cr(VI) could lead to health issues

doi:10.6342/NTU202401040

such as bronchitis, pneumonia, asthma, skin allergies, dermatitis, or perforated septum. Figure 1-3 shows the way of the mutagenicity of Cr(VI) and the pathway of DNA damage. Recognizing its significant health risks, Cr(VI) is classified as a major carcinogen by the World Health Organization (WHO).

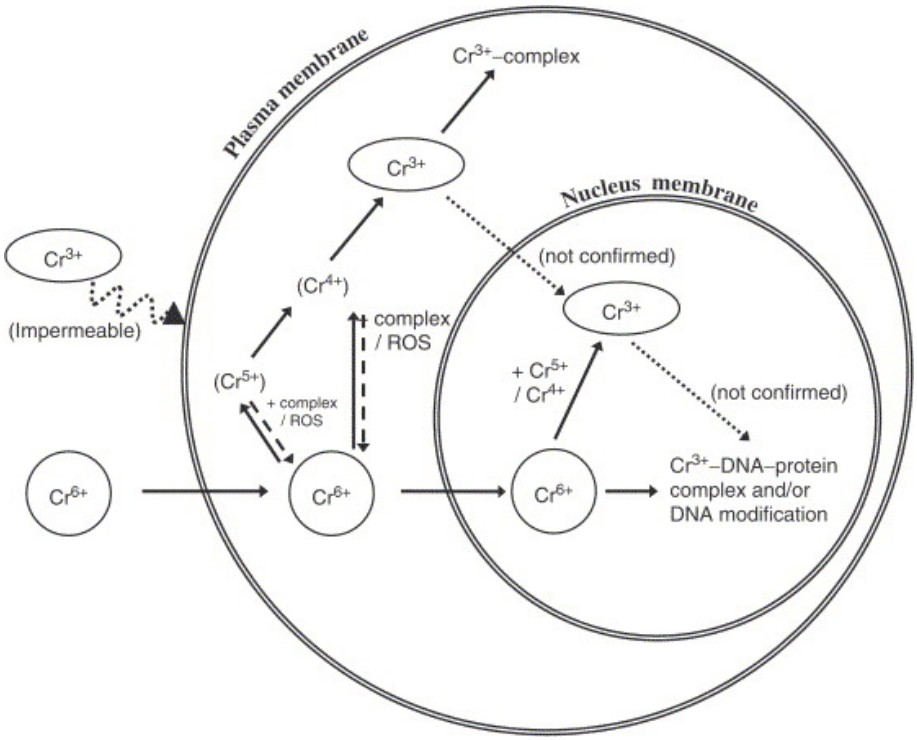

Figure 1-3 Diagram of toxicity and mutagenicity of Cr(VI) [4].

1.5 Current problems of Cr(VI) sensing

Although various cost-effective, portable, and stable sensing technologies are available for heavy metal ions sensing, traditional Cr(VI) methods still require skilled technicians to operate sophisticated analytical instruments within dedicated laboratories to obtain accurate results. Additionally, transporting samples from the target water source to the laboratory may introduce potential contamination to the samples. In the last two decades, some Cr(VI) sensing devices have been developed, but can only be processed in a narrow pH range and have difficulties distinguishing the signal of Cr(III) from Cr(VI). Other Cr(VI) sensing devices require complicated pre-processing, and harmful

doi:10.6342/NTU202401040

compounds may be used in these methods. Furthermore, few of them have the ability for real-time detection, not to mention the ability of automatic sensing under severe chemical conditions. To address the above issues, we aim to develop an easy-to-use, reliable, and portable device for automatic real-time sensing in various environments.

doi:10.6342/NTU202401040

Chapter 2 Literature review

2.1 Traditional Cr(VI) sensing methods

Traditional Cr(VI) sensing methods are (1) atomic absorption spectroscopy (AAS), (2) spectrophotometry, and (3) ion chromatography [5]. Atomic absorption spectroscopy is a commonly used technology for Cr(VI) sensing. The sample first undergoes ion separation, and the ion concentration in the gas phase is measured through light absorption. Ions in a stable state absorb energy from light at a specific wavelength, with the absorbed energy increasing alongside ion concentration. Comparing the amount of light absorbed by the sample with a standard allows for determining the known ion concentration. AAS typically measures total chromium, and if the goal is to measure Cr(III) and Cr(VI) separately, the sample needs pre-concentration or separation. Figure 2-1 (A) shows the schematic of the AAS system for metal ions sensing.

Flame atomic absorption spectrometry (FAAS) is the most commonly used technology for Cr(VI) sensing within AAS [6]. While FAAS offers sufficient precision and accuracy, it has low sensitivity and is easily interfered with by matrices. These issues could be addressed through a new method called on-line pre-concentration and separation system. By using suitable sorbent materials that maintain structure in most acid/alkaline environments and temperatures up to 180℃ [7], the method achieves a LOD of 2.0 μg/L. Electrothermal atomic absorption spectrometry (ETAAS) enhances sensitivity 2 to 3 times by eliminating the matrix before atomization and increasing the duration of sample atomization [8]. Graphite furnace atomic absorption (GFAAS), an AAS technology with an alternate heater using a graphite tube, allows most samples and matrices to be directly atomized to increase sensitivity and the LOD further.

Spectrophotometry measures the intensity of light absorption by the sample, with

doi:10.6342/NTU202401040

different chemical compounds exhibiting distinct absorption intensities and wavelength ranges. Various reagents, such as acidic Diphenylcarbazide (DPC) [9] and chromotropic acid (CA) [10], have been used to back-extract Cr(VI) for lower limits of detection. Ultraviolet spectrophotometric methods, such as those discussed by Noroozifar and Zhao et al. [11], offer alternative approaches to achieve low limits of detection. Figure 2-1 (B) shows the diagram of the X-ray spectrometer.

Ion chromatography scatters ions in the sample retains ions with atomic weights less than 500 using ion exchange resin and measures its conductivity. This method distinguishes anions, cations, and different oxidation states of ions [12].

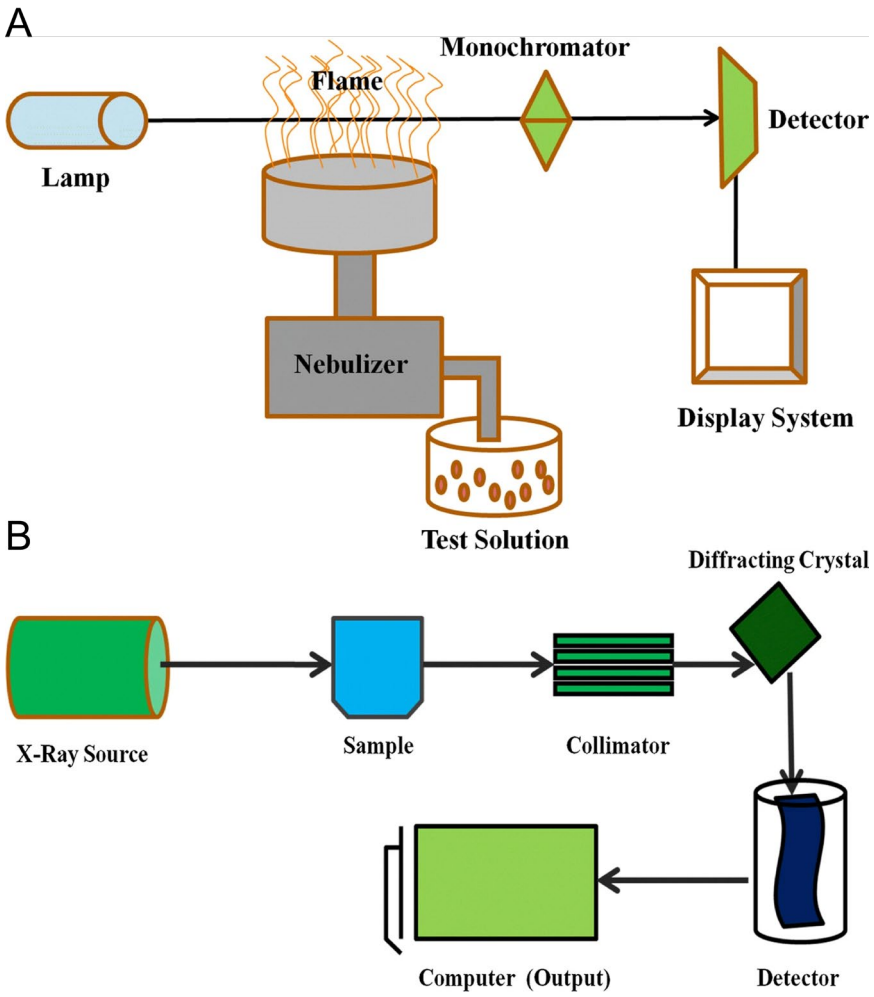

Figure 2-1 (A) Diagram of single-beam atomic absorption spectrophotometer, (B) Diagram of X-ray fluorescence spectrometer [13].

doi:10.6342/NTU202401040

2.2 Optical Cr(VI) sensing methods

Optical sensors represent a widely employed category among non-electrochemical sensors, relying on the target substance's emission or absorption of light. Recently, colorimetry has been developed for Cr(VI) monitoring. For Cr(VI) analysis, the ions are colored in the reactor by reacting with 1,5-Diphenylcarbazide and then analyzed by visible light with a wavelength of 550 nm. In acidic water samples, signal interference may occur if existing reducing substances transform Cr(VI) back to Cr(III) [14]. In a study by Nghia et al. [15], a colorimetric approach was developed. The oxidation of 3,3,5,5-tetramethylbenzidine (TMB) by H_2O_2, catalyzed by graphene oxide (GO), is influenced by the concentration of Cr(VI) through the interaction with 8-hydroxyquinoline (8-HQ). The resulting blue color from the oxidation reaction is detectable through spectrophotometry at 652 nm. Under optimal conditions, the linear range spans from 50 to 430 nM, with a LOD of 5.8 nM. In another study by Joshi et al. [16], a method utilizing flower-shaped silver nanoparticles (AgNPs) with 3,4-dihydroxyphenylalanine (L-dopa) as the reducing and stabilizing agent was reported for Cr(VI) detection. The presence of L-dopa around the AgNPs prevents aggregation, maintaining a dark yellow color in the solution. Cr(VI) in the sample solution undergoes self-reduction to Cr(V), causing oxidation of L-dopa, leading to AgNPs aggregation and a color change to reddish-brown. Detection is achieved through ultraviolet-visible (UV-Vis) spectroscopy, demonstrating a detection limit of 10^{-7} M.

2.3 Electrochemical Cr(VI) sensing methods

The electrochemical sensor presents a superior alternative to traditional methods due to the costliness and complexity of conventional instruments and setups. In electrochemistry, chemical reactions occur on the electrode, and the resulting electric

doi:10.6342/NTU202401040

charge passes through the sample solution (Figure 2-2). Electrochemical sensors offer several advantages in environmental analysis, including sample pre-processing reduction, time and cost reduction, and high sensitivity and selectivity maintenance. These sensors could generate signals for specific targets through chemical reactions and convert these signals into electrical signals for detection.

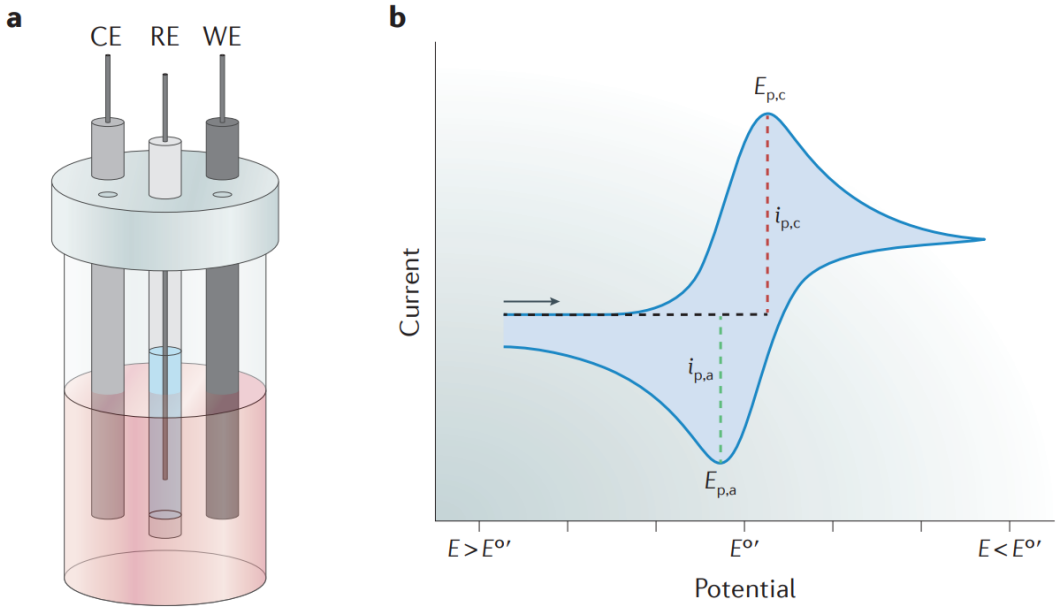

Figure 2-2 diagram of three-electrode sensor with a chart of a cyclic voltammogram [17].

2.3.1 Potentiometric sensor

The potentiometric sensor, commonly called ion-selective electrodes (ISEs), is suitable for real-time measurements owing to its short reaction time and simplified sample preparation. Potentiometry does not involve applying a voltage to the sample solution; instead, it solely measures its potential. The sensor captures the potential between the solution and the ion-selective membrane, which represents the difference in the affinity. The overall reaction involves a complex interaction among the solution, membrane, and interface, leading to various theoretical models under different circumstances. The solid chromium membrane has been the subject of extensive research, with the exploration of various ionophores such as C-thiophenecalix[4]resorcinarene [18], calix[4]arene

doi:10.6342/NTU202401040

derivatives [19], DABAm4 [20], β-diketone complex [21], Co(SALEN)2 [22], CuL2 [23], bis(acetylacetonato) Cd(II) [24], and others. However, these technologies still face limitations in real sample analysis, including low sensitivity to low concentrations of Cr(VI) ions and narrow requirements for pH and concentration ranges in working conditions. Additionally, certain materials are susceptible to interference from lipophilic anions like SCN-; some necessitate extended reaction times. In response to these challenges, several novel electrode types with new modifiers have been developed.

Solid selective membranes are the primary choice due to their high stability, aligning with the requirements of potentiometric sensors. Carbon paste electrodes (CPE) offer a stable signal, low resistance, and durability [25]. For instance, a CPE incorporating multi-walled carbon nanotubes (MWCNT) [26] exhibits a broad concentration detection range from 10^{-1} to 10^{-6} M and a sensitivity of 28.6 mV/decade. In a study by Prabhakaran et al. [27], a microbial sensor for the voltammetric detection of chromium was developed utilizing a CPE modified with Citrobacter freundii. The LOD for Cr(VI) and Cr(III) was determined to be 1×10^{-4} M and 5×10^{-4} M, respectively.

Recently, several innovative compounds have demonstrated the capability for sensing Cr(VI) with high sensitivity and low LOD. Yenpei's research team utilized a nanostructured shuriken $BiVO_4$ [28] in electrochemical Cr(VI) sensing (Figure 2-3), achieving a detection range of 0.01 to 264.5 μM and a low LOD of 3.5 nM. Notably, $BiVO_4$ exhibited excellent stability and recovery in real sample tests. Magnetic graphene oxide (GO) [29, 30], a two-dimensional electrical material, has gained prominence as an analytical material due to its extremely high specific surface area and adsorption capacity on both sides of graphite. Due to its distinct affinity for Cr(III) and Cr(VI), it enables the detection, separation, and extraction of samples in specific situations. The detection range for this material is from 0.5 to 50.0 μg/L, with an LOD of 0.1 μg/L.

doi:10.6342/NTU202401040

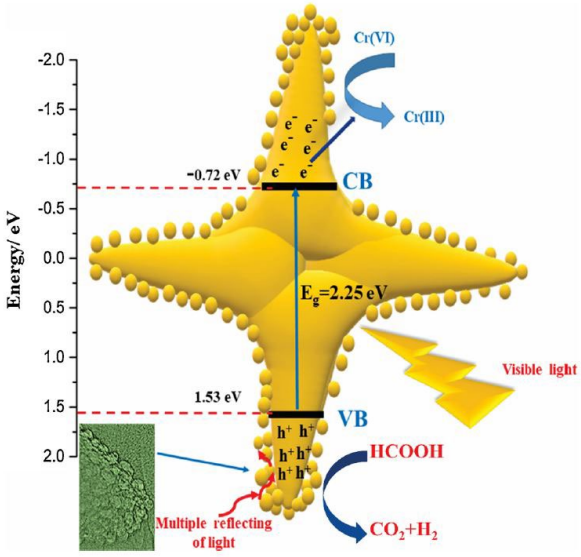

Figure 2-3 Diagram for the Cr(VI) reduction using shuriken $BiVO_4$ [28].

A recent advancement involves a photoelectrochemical sensor [31], employing $Pb_5S_2I_6$ as a photocatalyst coated on porous TiO_2. This technology demonstrates a sensitivity of 1.9 μA/μM, a great LOD of 3.0 nM, and a relatively wide detection range from 0.01 to 80 μM. Yari et al. [32] introduced a PVC ion-selective membrane (ISM) electrode utilizing a novel material named Quinaldine Red as an ionophore for Cr(VI) detection. The linear range spans from 5.2×10^{-6} M to 1.0×10^{-1} M. Additionally, Shahim et al. [33] presented a device incorporating Quinaldine Red mixed in a PVC-ISM combined with extended-gate field-effect transistors (EGFETs) for Cr(VI) and Cr(III) sensing (Figure 2-4 (A)). This approach utilizes the change in resistance of ISM due to the chemical reaction with different concentrations of Cr(VI) to modify the final signal received by the FETs. The linear range of their device extends from 10^{-6} to 10^{-4} M, with a LOD of 10^{-6} M.

The potentiometric biosensor typically comprises a bio-signal detection element and an energy transformation element, with the potential signal serving as the final output. The working electrode could be modified using various chemical compounds or biomedical technologies. One prevalent technology in this domain is the microbial fuel

doi:10.6342/NTU202401040

cell (MFC) (Figure 2-4 (B)). MFC offers several advantages, including distinct responses to different shocks, rapid response times, the ability to generate power from wastewater without external energy sources, and the absence of the need for external enzymes. A noteworthy example is the self-recovering MFC [34], which utilizes Plexiglas as its single-chamber batch-mod cube material. The cathode is constructed from a four-layer polytetrafluoroethylene (PTFE) and carbon cloth. This MFC demonstrates the ability to differentiate between toxic and non-toxic shocks by controlling the voltage signal, and the entire sensor could resume operation after 65 hours.

Two-chamber microbial fuel cells (MFCs) [35], crafted from acrylic, have also been applied for the measurement of Cr(VI). The anode and cathode are compressed at 140 °C to form a membrane electrode assembly. In an alkaline environment, when Cr(VI) falls within the range of 10 to 300 mM, the voltage of the MFCs undergoes significant changes with increasing concentration. However, the signal diminishes considerably as the pH level rises.

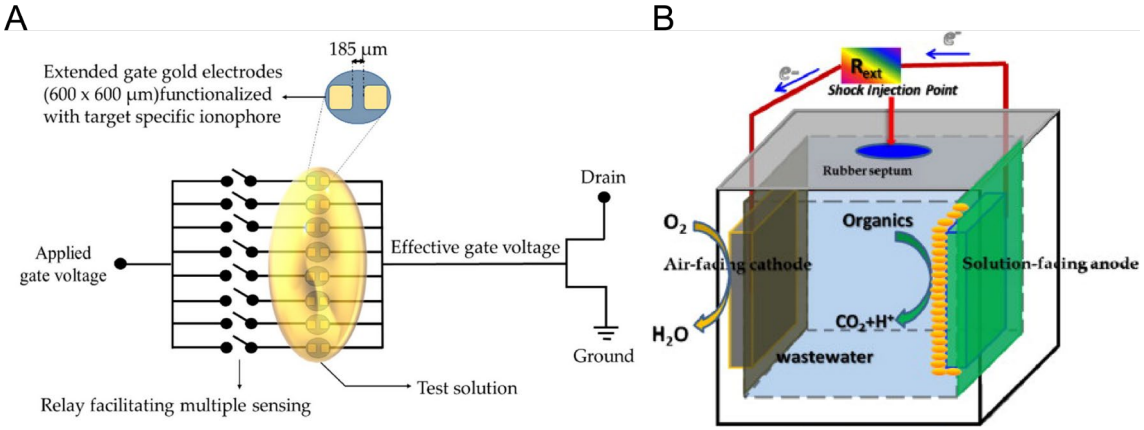

Figure 2-4 (A) Schematic of extended-gate field effect transistors sensor system [33], (B) Schematic of the single chamber cube microbial fuel cell (CMFC) [34].

2.3.2 Amperometric sensor

Amperometric technology involves applying a fixed or dynamically changing

doi:10.6342/NTU202401040

voltage to the sample solution and measuring the resulting change in redox current. As the reaction encompasses electron transformation, an amperometric device typically comprises a voltage generator element and a dual-electrode system soaked in an appropriate electrolyte. Voltammetry is the most commonly employed technology in this context. Among the various voltammetry technologies for Cr(VI) measurement, catalytic adsorptive stripping voltammetry (CAdSV) stands out as the highest sensitive and practical measurement. CAdSV exhibits an exceptionally low limit of detection and the capability to measure Cr(VI) directly. Jorge et al. [36] utilized the rotating-disc bismuth film electrode to measure Cr(VI) in DTPA, achieving a LOD of 0.336 nM. Additionally, Grabarczyk [37] introduced a novel protocol that allows CAdSV to extract and measure total chromium from samples within the pH range of 5.0-6.0. While most of the mentioned research operates in environments with a pH ≥ 2, there is still considerable interest in developing new technologies capable of measuring Cr(VI) in strong acid environments.

Screen-printing emerges as an innovative solution to address the challenges above. This technique allows for the mass production of affordable, stable, single-use sensors. These disposable sensors prove effective for Cr(VI) detection in strong acid environments. Screen-printed electrodes (SPE) are created by repeatedly printing specific materials onto ceramics or plastic substrates (Figure 2-5).

Successful research has already demonstrated the measurement of Cr(VI) in sulfuric acid using SPE. The electrodes, constructed through multiple printings on an aluminum oxide substrate, exhibit a broad dynamic range from 3 to 40 mmol/L, with a linear range from 3 to 10 mmol/L. The slope is 0.08 mA/mM, and the LOD is 1 μmol/L. Wang et al. [38] developed a carbon nanotube (CNT)-based SPE for electrochemical Cr(VI) sensing through amperometry, achieving a low limit of detection of 2×10^{-7} M when using a large

doi:10.6342/NTU202401040

area electrode. The CNT-SPE demonstrates excellent selectivity for Cr(VI) and performs effectively in detecting the target in cooling tower blowdown water.

The development of silver (Ag) has increased due to its excellent conductivity and catalytic performance. Stonajovic et al. [39] introduced a novel technology employing a silver-plated glassy carbon electrode (Ag plated-GCE) for measuring Cr(VI) with differential pulse anodic stripping voltammetry (DP-ASV). The calibration curve's linear range at pH 5.9 spans from 0.35 to 40 μM, with LOD as low as 0.1 μM.

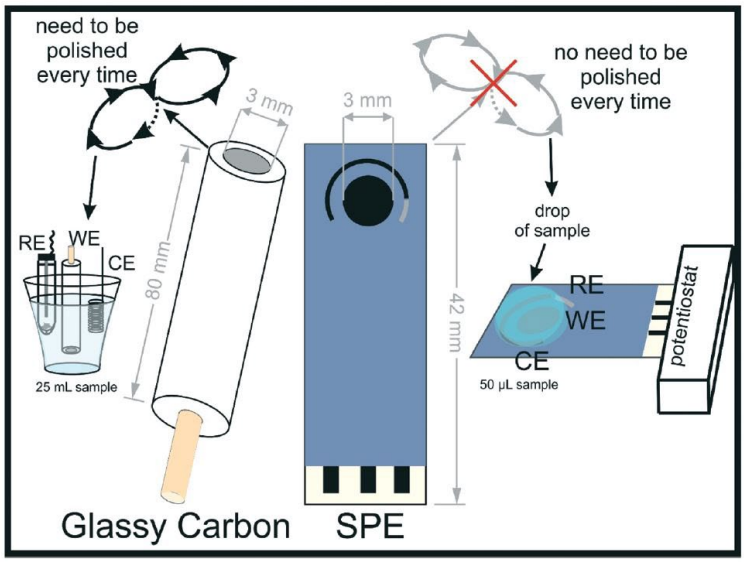

Figure 2-5 Comparison of classic electrochemical cell and screen-printed electrode platform [40].

2.4 Summary of current Cr(VI) sensing methods

Individuals have employed diverse methodologies to detect the ppm to ppb range of heavy metal ions in water, with continuous efforts spanning the past few decades. Advanced analytical instruments, including atomic absorption spectroscopy, spectrophotometry, and ion chromatography, have demonstrated exceptional performance in accurately identifying heavy metal ions at concentrations below ppb. Nevertheless, these methods exhibit several drawbacks, encompassing a lack of portability, high cost,

doi:10.6342/NTU202401040

prolonged analysis times, the necessity for pre-processing steps, dependence on skilled operators, and ongoing maintenance requirements. Additionally, the precision achieved by these methods mandates expensive and intricate instrumentation, increasing the difficulty of on-site detection.

Optical sensors for heavy metal ions involve detecting optical changes generated by interactions between targets and recognizing elements at the input end. These changes aid in determining the concentration of target ions. However, these sensors necessitate continuous sensing, requiring human operation each time the sensor reaction is monitored, thereby adding to the complexity of use. Certain electrochemical methods, such as voltammetry and amperometry, have proven successful in detecting heavy metal ions through sensor applications. However, these sensors encounter challenges in frequent on-site determinations. Colorimetry serves as a widely utilized sensing technology for heavy metal ion detection. It relies on color changes resulting from chemical reactions between target ions and elements. The advantage of colorimetric sensors for heavy metal ions lies in their ability to detect different target ions simultaneously. However, due to the irreversibility of most colorimetric analysis reactions, sensors based on colorimetry are typically disposable for one-time use in heavy metal ion measurement. Consequently, these methods have difficulty for continuous and stable monitoring.

Table 1 shows several types of research mentioned in this chapter. As shown in the table, optical methods have a better limit of detection while having a narrow linear range and relatively long response time; electrochemical methods have a better linear range and shorter response time, but many of them require a large amount of dosage of the target solution. Also, the fabrication of electrodes and modifiers required complicated preparation.

doi:10.6342/NTU202401040

2.5 Research Motivation

While the aforementioned sensing methods offer cost-effectiveness and user-friendliness, providing high sensitivity, selectivity, and stability in heavy metal ion analysis within laboratory settings, there is a growing demand for portable, rapid sensors for on-site detection. Semiconductor-based sensors possess outstanding characteristics, including portable, real-time response, great sensitivity, and well-fabricated suitable for on-site measurement. These sensors could be manufactured using mature semiconductor industry technologies. Among all of them, ion-sensitive field-effect transistors (ISFET) have appeared in various applications, except for chromium atoms. The operational principle of ISFET sensors involves transducing and monitoring changes induced by the absorption material in channel conductivity variations, which could be reflected through the current from drain to source. Various studies are underway to develop ISFET for detecting heavy metal ions in water.

There are already lots of modifiers integrating ISFET for ion sensing have been developed. Nevertheless, the connection between the ISFET surface and modifier was usually accomplished by a covalent bond, resulting in a non-reusable ISFET body, which is a serious disadvantage against disposable screen-printed electrodes. Therefore, PVC-based porous ion-selective membrane (ISM) has been chosen for this research. The Fast-forming and easy-to-remove characteristics of PVC-ISM exactly hit the need for the shortcomings mentioned above. Therefore, this paper primarily presents research results utilizing ISFETs, with PVC-ISM and a specific ionophore serving as the Cr(VI) ion sensor.

doi:10.6342/NTU202401040

Table 1 Comparison of different electrochemical methods for Cr(VI) ion measurement

Method	electrode	modifier	Linear range (M)	Detection of limit (M)	Sensitivity	Response time (min)	Dosage of target	Reference
Optical	graphite oxide Nanoparticle		5×10^{-8}–4.3×10^{-7}	5.8×10^{-9}	78 μM^{-1} (Absorbance)	60	200 µL	[15]
Optical	Ag-Nanoparticle		10^{-7}–10^{-4}	1×10^{-7}	1 μM^{-1} (Absorbance)	20	200 µL	[16]
Potentiometry	Ag/AgCl	Calix [4] arene derivatives	10^{-5}–10^{-2}	6.2×10^{-7}	53 mV $\log(M)^{-1}$	1	25 mL	[19]
Potentiometry	Ag/AgCl	Rhodamine-B	5×10^{-5}–10^{-1}	1×10^{-6}	30 mV $\log(M)^{-1}$	1	50 mL	[41]
Potentiometry	Ag/AgCl	Quinaldine red	5.2×10^{-5}–10^{-1}	2.5×10^{-6}	56 mV $\log(M)^{-1}$	1	50 mL	[32]
Potentiometry	carbon paste electrode	Citrobacter freundii	10^{-7}–10^{-4}	1×10^{-7}	0.6 µA $\log(M)^{-1}$	4	20 µL	[27]
Potentiometry	Acetate oxidation		10^{-6}–1.5×10^{-4}	1×10^{-6}	3.3×10^{-6} mV M^{-1}	120	120 mL	[35]
Amperometry	screen-printed electrode	Carbon-nanotube	2×10^{-7}–10^{-5}	2×10^{-7}	0.6 A M^{-1}	4	20 mL	[38]
Amperometry	glassy carbon electrode	Ag	3.5×10^{-7}–4×10^{-5}	1×10^{-7}	1.59 A M^{-1}	2-4	5 mL	[39]

doi:10.6342/NTU202401040

Chapter 3 Experimental Design

3.1 The principle of dual-gate ion-sensitive field-effect transistor (ISFET)

The ISFET was remodeled from MOSFET (Metal-Oxide-Semiconductor Field-Effect Transistor). It had three major elements called Gate, Drain, and Source (Figure 3-1 (a)). The drain current I_D flowed from drain to source would be controlled by the applying voltage on the gate V_{gs} minus a fixed number called threshold voltage V_{th} (Figure 3-1(c)). ISFET took off the metal on the gate and replaced it with electrolyte solution and reference electrode (Figure 3-1(b)), the condition of electrolyte solution (pH, ionic strength, etc.) became the control elements of applied voltage V_{gs}, and the change of drain current I_D could further detect.

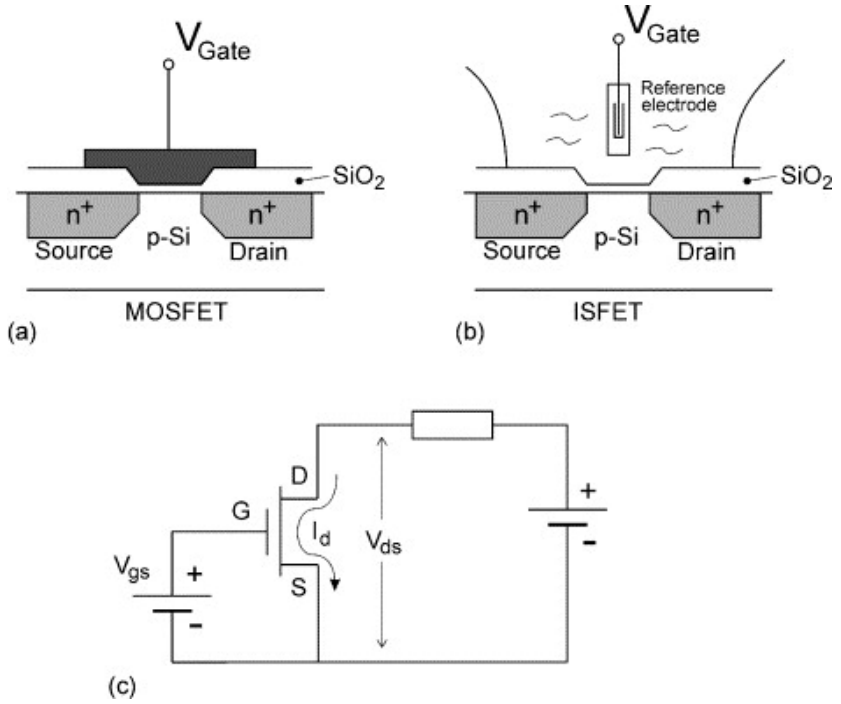

Figure 3-1 Schematic representation of (a) MOSFET; (b) ISFET; (c) and electronic diagram [42].

Before explaining the principle of ISFET, we should introduce the surface material

doi:10.6342/NTU202401040

used for the gate of ISFET: amphoteric metal. Amphoteric metals confirmed usable, including SiO_2, Ta_2O_5, Si_3N_4, Al_2O_3, and HfO_2. These materials have amphoteric surface sites (Figure 3-2), which means that the surface metal serves as proton donors or acceptors:

$$A-OH \overset{K_a}{\Leftrightarrow} A-O^- + H_s^+ \tag{1}$$

$$A-OH + H_s^+ \overset{k_b}{\Leftrightarrow} A-OH_2^+ \tag{2}$$

and the dissociation constants are:

$$K_a = \frac{[A-O^-][H_s^+]}{[A-OH]} \tag{3}$$

$$K_b = \frac{[A-OH_2^+]}{[A-OH][H_s^+]} \tag{4}$$

$[A-O^-]$, $[A-O^-]$ and $[A-OH_2^+]$ are the number of neutral sites, negative and positive surface groups per cm^2. $[H_s^+]$ represents the number of protonated water molecules, $[H_3O^+]$. Combine two equations above, we could get:

$$[H_s^+]^2 = \frac{K_a}{K_b}\frac{[A-OH_2^+]}{[A-O^-]} \tag{5}$$

and we could get the following equation for a neutral surface:

$$[H_s^+] = \sqrt{\frac{K_a}{K_b}} \tag{6}$$

or

$$pH_s = -\log[H_s^+] = -\log\sqrt{\frac{K_a}{K_b}} \tag{7}$$

The terms pH_s and pH_b represent the pH of the solution near the metal surface and bulk solution, respectively. Under neutral conditions, they are equal. When pH_b changes significantly, the amphoteric surface sites on the surface of the amphoteric material can exhibit a buffering effect, reducing both the magnitude and the rate of change

doi:10.6342/NTU202401040

of pH_s. This reaction can be quantified in terms of the intrinsic buffer capacity of the surface, β_s, which is defined as the ratio between a small amount of strong base or acid, d[B], and the resulting change in pH, dpH_s:

$$\beta_s = \frac{d[\mathrm{B}]}{dpH_s} \tag{8}$$

$$[\mathrm{B}] = [A - O^-] - [A - OH_2^+] = -\frac{\sigma_s}{q} \tag{9}$$

where σ_s is the net surface charge of the groups per cm^2 and $q = 1.6 \times 10^{-19}$C.

Because of the existence of β_s, pH_s will not follow the number of pH_b immediately. During this process, a surface potential ψ_0 would be generated. According to the Boltzmann distribution:

$$\psi_0 = 2.3\frac{kT}{q}(pH_s - pH_b) \tag{10}$$

it would charge the electrical surface capacitance C_s :

$$\sigma_s = -\psi_0 C_s \tag{11}$$

according to equations (8), (9) and (11):

$$\frac{d\psi_0}{dpH_s} = \frac{d\sigma_s}{dpH_s}\frac{d\psi_0}{d\sigma_s} = \frac{-q\beta_s}{C_s} \tag{12}$$

so, we could derive from equation (12) how the surface potential ψ_0 changes when we change the pH of bulk solution pH_b:

$$\frac{d\psi_0}{dpH_b} = 2.3\frac{kT}{q}\left(\frac{dpH_s}{dpH_b} - 1\right)$$

$$= 2.3\frac{kT}{q}\left(\frac{dpH_s}{d\psi_0}\frac{d\psi_0}{dpH_b} - 1\right)$$

$$\Rightarrow \frac{d\psi_0}{dpH_b} = \frac{2.3\frac{kT}{q}}{2.3\frac{kT}{q}\cdot\frac{dpH_s}{d\psi_0} - 1} \tag{13}$$

combining equations (12) and (13) results in:

doi:10.6342/NTU202401040

$$\frac{d\psi_0}{dpH_b} = -2.3\frac{kT}{q}\cdot\left(\frac{1}{2.3\frac{kT}{q^2}\cdot\frac{C_s}{\beta_s}+1}\right) = -2.3\alpha\frac{kT}{q} \quad (14)$$

in this way, the influence to ψ_0 from changing pH_b would be decided by intrinsic buffer capacity β_s and electrical surface capacitance C_s.

The drain current of a MOSFET in triode mode is:

$$I_D = \mu C'_{ox}\frac{W}{L}[(V_{GS}-V_{th})V_{DS}-\frac{1}{2}{V_{DS}}^2] \quad (15)$$

where μ is the effective surface mobility, C'_{ox} is the oxide capacitance per unit area, W and L are the channel width and length, and V_{GS}, V_{th}, and V_{DS} are the gate-to-source, threshold, and drain-to-source voltage.

The usual V_{th} is:

$$V_{th} = \left(\frac{\Phi_M-\Phi_{Si}}{q}-\frac{Q'_{ox}}{C'_{ox}}\right)+2\phi_{FB}-\frac{Q'_B}{C'_{ox}} \quad (16)$$

where the Φ_M and Φ_{Si} refer to the metal-semiconductor work function, ϕ_{FB} is the Fermi potential of the silicon, Q'_{ox} is the oxide trapped charge per unit area, and Q'_B is the depletion charge per unit area.

ISFET could be seen as a modified version of MOSFET. The metal gate is replaced by the reference electrode and the analyzed electrolyte. Also, two new terms have to be considered. they are the reference electrode potential E_{ref} and the interfacial potential at the electrolyte-insulator interface ψ_0 and χ_{sol}. Both E_{ref} and χ_{sol} are fixed coefficients, so the equation 16 could be rewritten as:

$$V_{th} = \left(E_{ref}+\chi_{sol}-\psi_0(\mathrm{pH})--\frac{\Phi_{Si}}{q}-\frac{Q'_{ox}}{C'_{ox}}\right)+2\phi_{FB}-\frac{Q'_B}{C'_{ox}} \quad (17)$$

therefore, the relationship between ISFET signal I_D and pH_b could be fully illustrated by equation (14) and (17).

The dual-gate ISFET produced by Taiwan Semiconductor Manufacturing Corp.

doi:10.6342/NTU202401040

(TSMC) could improve the drifting and hysteresis effect that happened on the traditional ISFET. The dual-gate ISFET has an additional oxide layer on the body side called the back gate; the reference electrode is called the fluidic gate. The signal would be balanced by the capacitive-coupling effect between the fluidic and back gate, improving the stability of the response.

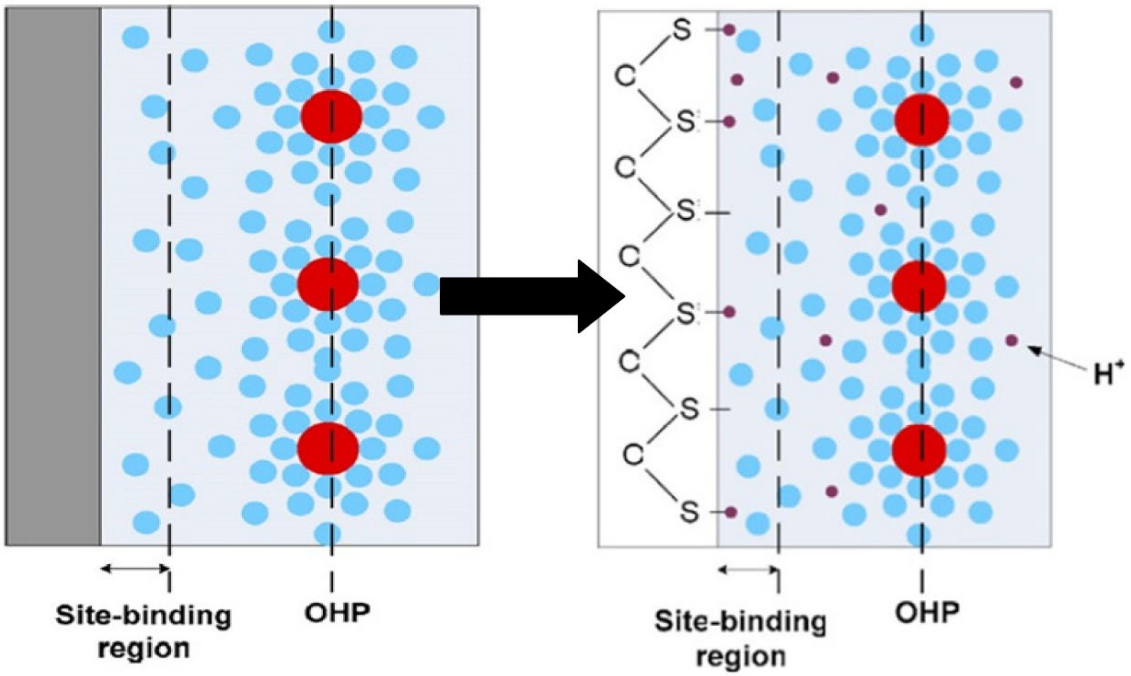

Figure 3-2 Site-dissociation and binding model representation of amphoteric metal surface [43].

3.2 The principle of ISM

ISM has been commonly used in different types of sensors ranging from electrical potentiometers, ISE, or ISFET to optical. There are many types of ISM, such as glass, solid-state, and liquid-state [44, 45]. Typically, the composition of a PVC-based ion-selective membrane comprises an ionophore, ion exchanger, polymer matrix with plasticizer, and mixed with a volatile solvent, commonly tetrahydrofuran (THF). When the THF in the membrane evaporates, a plastic polymer layer will ultimately form.

The ionophore is the reason why ISM can be selective. In Cr(VI) ISM, the ionophore

doi:10.6342/NTU202401040

is Quinaldine Red (2-(4-dimethylaminostyryl)-1-ethylquinoliniumiodide) (Figure 3-3), which has a strong signal change with Cr(VI) anions in the absorption of the solution at 350 nm and 520 nm [32], to act as a suitable ionophore for Cr(VI) anions in PVC membrane. Wang et al. also report a significant change of potential drop across the membrane after the contact of Cr(VI) solution [33], making Quinaldine Red a great choice for forming Cr(VI) captured membrane. The Cr(VI) ISM acts like a special kind of ion-exchange membrane: it only stops Cr(VI) anions from passing through the membrane; any other ions in the solution could travel through the membrane easily. This behavior resembles the Gibbs-Donnan effect (Figure 3-4) [46]. To maintain electrical neutrality, a sufficient number of counter-ions are required to neutralize the fixed charge, thus generating a significant electrical "Donnan" potential to preserve electrical neutrality

In our case, the Cr(VI) ions would be captured into the ISM and could not pass through it towards the surface of the sensor, leading to a Donnan potential due to the concentration difference of solution at opposite sides of the ISM.

For a membrane-solution interface, the Donnan effect confirms the equation [47]:

$$\psi_D = \frac{\mu_I^{0,aq} - \mu_I^{0,mem}}{F} + \frac{RT}{z_I F} \ln \frac{a_I^{aq}}{a_I^{mem}} \tag{18}$$

where ψ_D is the Donnan potential, $\mu_I^{0,aq}, \mu_I^{0,mem}$ and $a_I^{0,aq}, a_I^{mem}$ are the standard chemical potentials and the activities of ion in aqueous and membrane phase, z_I is the ion charge, F is the Faraday constant, R is the gas constant and T is temperature.

For an ISM having an aqueous solution at both sides, the potential drop across the whole ISM could be written as:

$$\psi_{ISM} = {\psi_{ISM}}^0 + \frac{RT}{z_I F} ln \frac{a_I^{aq}(1)}{a_I^{aq}(2)} \tag{19}$$

where ψ_{ISM} is the potential drop crossing the ISM, $a_I^{aq}(1)$ and $a_I^{aq}(2)$ are the

doi:10.6342/NTU202401040

activities of I^{z_I} analyte ion in the opposite side of the solution. The ψ_{ISM} increases with the increase of analyte ions and the capturing efficiency of ISM.

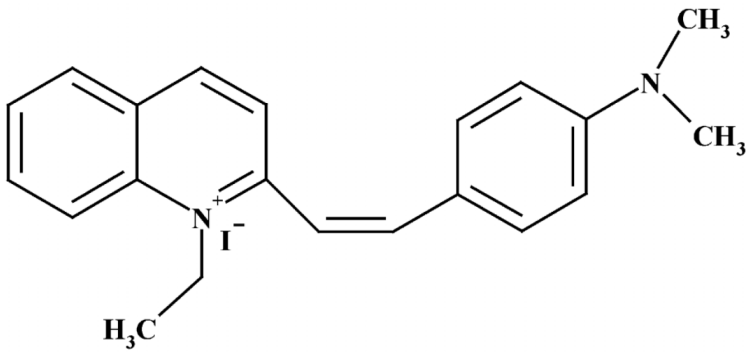

Figure 3-3 Chemical structure of Quinaldine Red [32].

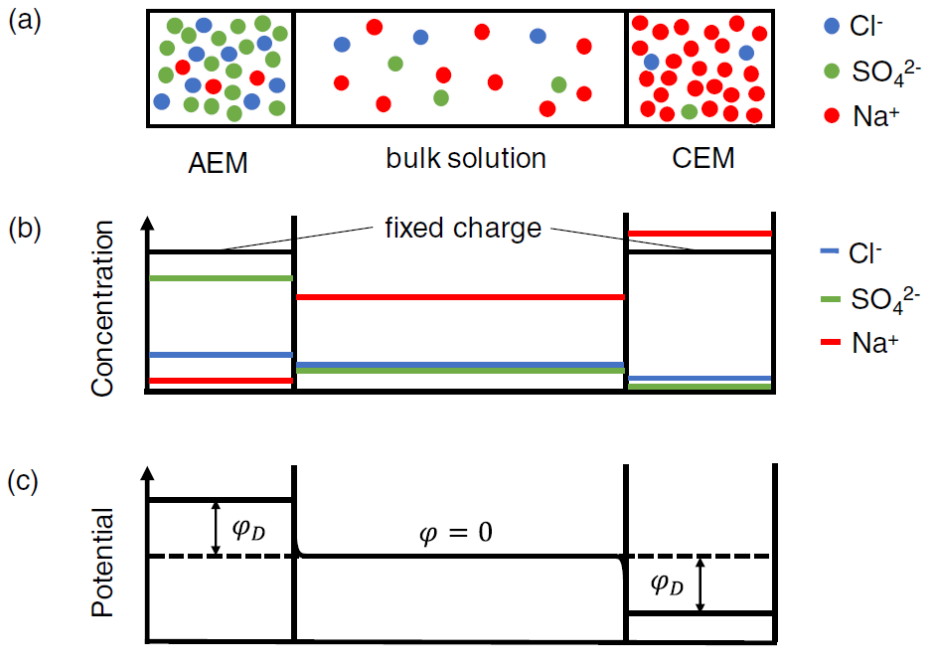

Figure 3-4 (a, b) Diagram of ion concentration between membranes and solution. AEM and CEM stand for anion-exchange and cation-exchange membranes. (c) shows the Donnan potentials (ψ_D) at the interfaces. [46]

3.3 The working principle of ISM-ISFET

Figure 3-5 depicts a model illustrating the distribution of electrostatic potential across an ISM-ISFET structure under a bias V_a. Within this structure, several potential

doi:10.6342/NTU202401040

drops can be observed [48]:

1. Potential drop at the electrode-electrolyte interface $\mathrm{E}_{ref} + \chi_{sol} - \chi_M$.
2. Potential drop across the Cr(VI) ISM ψ_{ISM}.
3. Potential drop at the electrolyte-insulator interface ψ_0, which was mentioned earlier in section Chapter 3.
4. Potential drop within the insulator ψ_{ox}.
5. Potential drop in the semiconductor ψ_s.
6. Potential drop between the semiconductor-metal interface $\chi_M - W^{Si}$

There is no current in the structure when the whole system is balanced. So we can combine all the constant forms (not a function of V_a) into a single component V_{FB}:

$$V_{FB} = \mathrm{E}_{ref} + \chi_{sol} - \chi_M + \chi_M - W^{Si} \tag{20}$$

so we could write the following equation:

$$V_a = V_{FB} + (\psi_{ISM} + \psi_0) + (\psi_{ox} + \psi_s) \tag{21}$$

under constant bias, the change of ψ_{ISM} due to the increase of Cr(VI) in the sample solution will break the electrochemical equilibrium in the electrolyte solution, leading to the change of surface potential ψ_0. This will eventually enforce a change of $(\psi_{ox} + \psi_s)$, and the electronic channel will be changed and finally modulate the current I_D.

However, the change of other ions in the solution will also influence the surface potential ψ_0 by changing the pH of the solution. This will cause a misreading of the final signal. To avoid that, we developed a sensing process called “Differential sensing.”

The area of the ISFET sensing array consists of 32 × 32 pixels, allowing multiple sensing in the maximum of 4 pixels. We covered only half of the ISFET sensing array with Cr(VI) ISM, leaving the left half area uncovered (no ISM). In this way, the signal of Cr(VI) covered area Sig_{CrISM} could measure both the change of $(\psi_{ISM} + \psi_0)$ from

doi:10.6342/NTU202401040

Cr(VI) anions and other ions, while the signal of uncovered area Sig_{noISM} could only detect the change of ψ_0 from other ions.

The differential signal Sig_{diff} defined as follows:

$$Sig_{diff} = Sig_{noISM} - Sig_{CrISM} \quad (22)$$

represents the signal response detected by ISM-ISFET from only the change of ψ_{ISM} influenced by the change of Cr(VI) concentration.

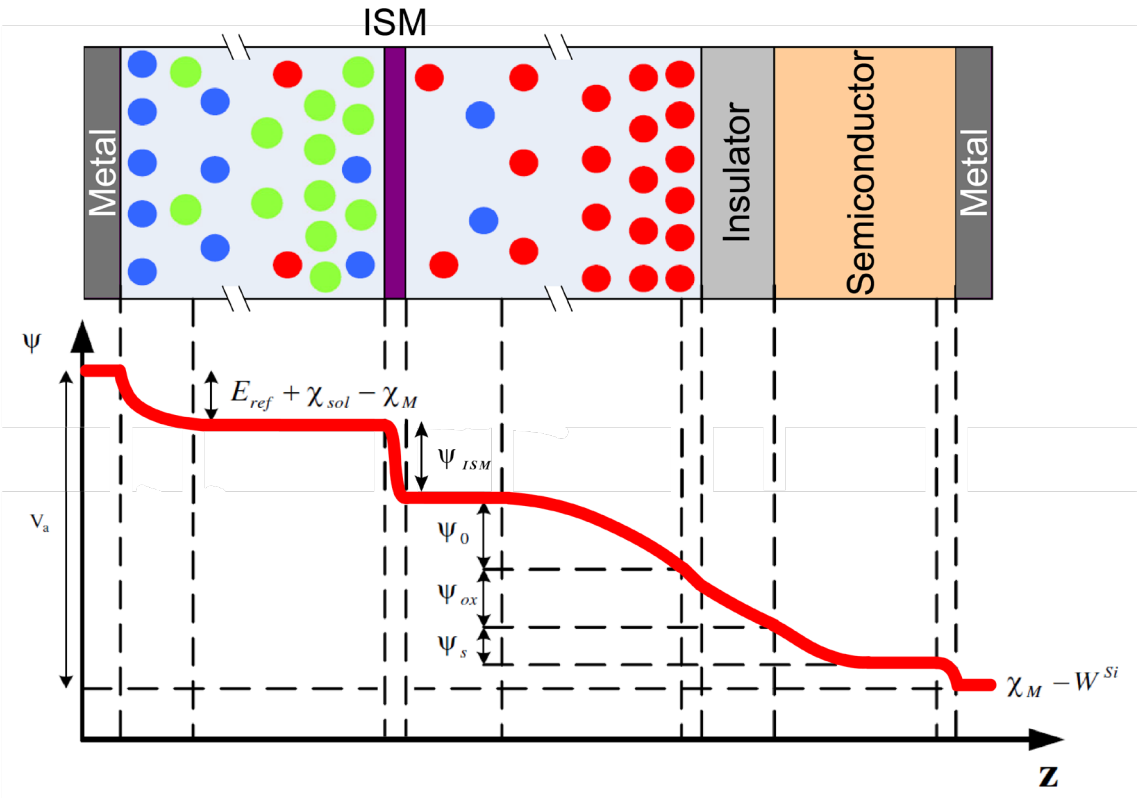

Figure 3-5 Potential drops along the ISM-ISFET structure. The colored ions are: Cr(VI) anions(green), other ions(red and blue) (modified from [48]).

doi:10.6342/NTU202401040

Chapter 4 Materials and methods

In this chapter, we would introduce the experiment setup, including a portable ISFET reader, pressure pump system, DG-ISFET, and microchannel. Then, we would explain how to operate the pressure pump system to meet the requirement of automatic regular measurements. After that, we would introduce the production method of each project item. Finally, we would introduce the preparation of the standard solution, Cr(VI) ISM solution, and ditch water.

4.1 Experimental setup

The whole Cr(VI) detection system could be separated into three parts: (1) A portable and real-time measuring reader for continuously recording the signals (Figure 4-1 (A)), (2) A PMMA-based microchannel integrated with ISM-ISFET (Figure 4-1 (B)), (3) The pressure pump system consist of a touchscreen displayer, a Raspberry Pi computer and two pressure pumps (Figure 4-1 (C)). As shown in Figure 4-1 (D), The area of the ISFET sensor consists of 32 × 32 pixels, which was part-covered with Cr(VI) ISM, leaving the left half area uncovered (no ISM). Figure 4-1 (E) shows the microchannel's parts breakdown. The volume of the channel is 85 μL, the sensing chamber is 200 μL, and the waste trench is 2 mL. Figure 4-1 (F) shows the whole system setup, with the combination of the three parts mentioned above and the connection between the pressure pump system and microchannel using Tygon tubes for transportation of sample and buffer solution.

doi:10.6342/NTU202401040

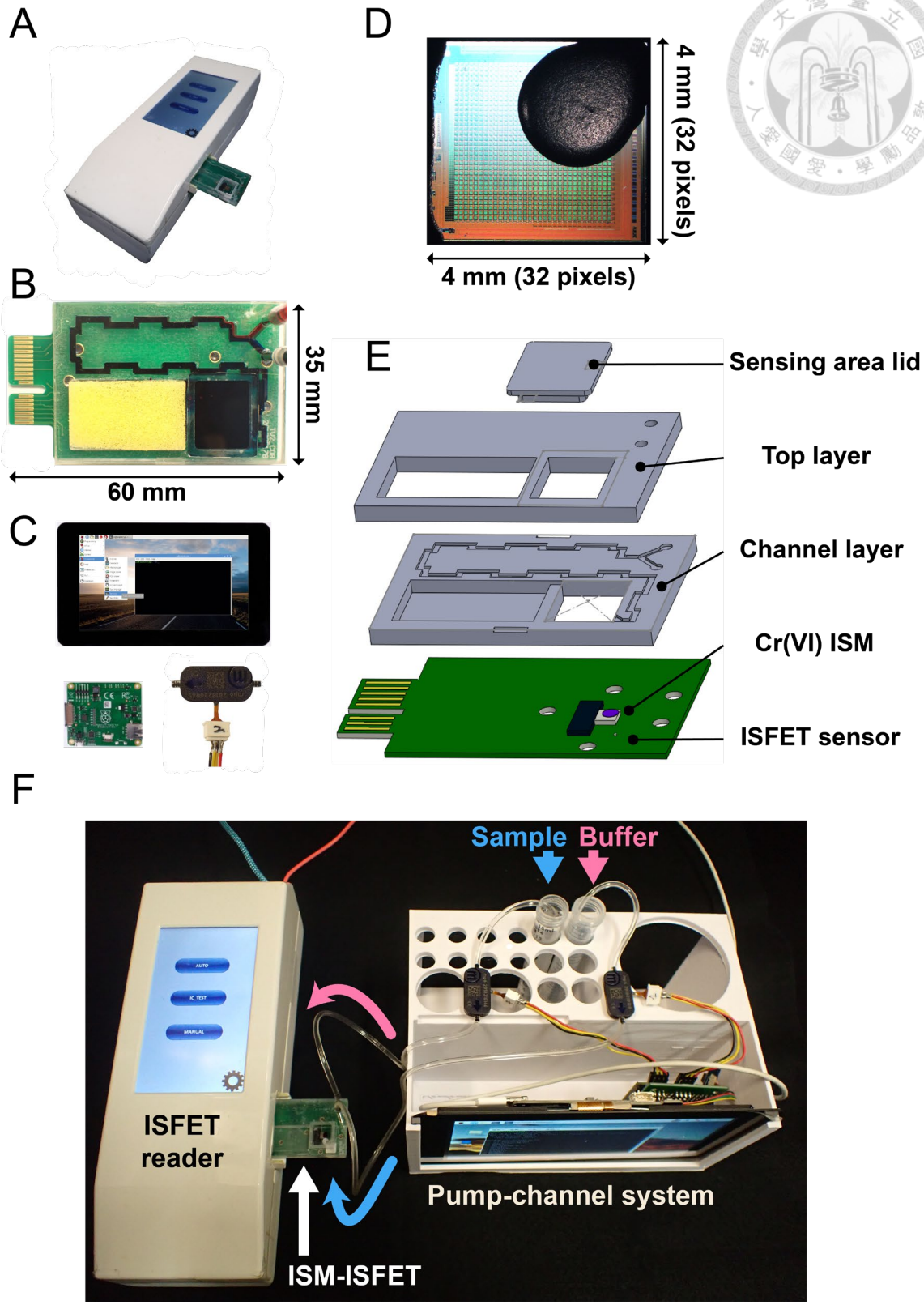

Figure 4-1 (A) The image of the ISFET reader, (B) The image of the ISM-ISFET with a dimension of 60 mm × 35 mm, (C) The photograph of a 7 inch touchscreen displayer, a

doi:10.6342/NTU202401040

Raspberry Pi computer, and a pressure pump, (D) a Microscopic image of the ISFET deposited Cr(VI) ISM, the dimension of sensing area is 4 mm × 4 mm, (E) Schematic of the PMMA-based microchannel integrated with ISM-ISFET, which consists of (1) small sensing area lid; (2) top cover layer; (3) channel layer for mixing sample and buffer; (4) ISM-ISFET made of PCB board; (F) the photograph of whole system setup.

4.2 Operation procedures of the experiment

4.2.1 Operation procedures of the microfluidic platform

Figure 4-2 shows the schematics of the whole system. Before the measurement started, the sensing area was filled fully with the corresponding baseline solution for 30 min to moisten the ISM and the surface of ISFET. The portable reader would keep recording the signal during the whole measurement. The operation protocol is shown as follows.

1. Buffer loading step: the buffer-side pressure pump was turned on for 3 minutes. 1.5 mL of buffer solution would flow through the sensing area. Then, the pump would be turned off for 3 min baseline calibration.
2. Sample loading step: both pressure pumps (including sample-side and buffer-side) would be turned on for 3 min. 3 mL of sample and PBS buffer solution (1:1) would be mixed through the microchannel and then flow through the sensing area. Then, both pumps would be turned off for 3 min sample detection.
3. Repeating step: if further measurement is needed, the buffer-side pressure pump would be turned on for 3 min again to wash off the mixed solution in the microchannel and the sensing area. After that, the pump would be turned off for another 3 min baseline calibration. All of the operations of the pressure pump system could be pre-written in the Raspberry Pi computer for automatic measurement.

doi:10.6342/NTU202401040

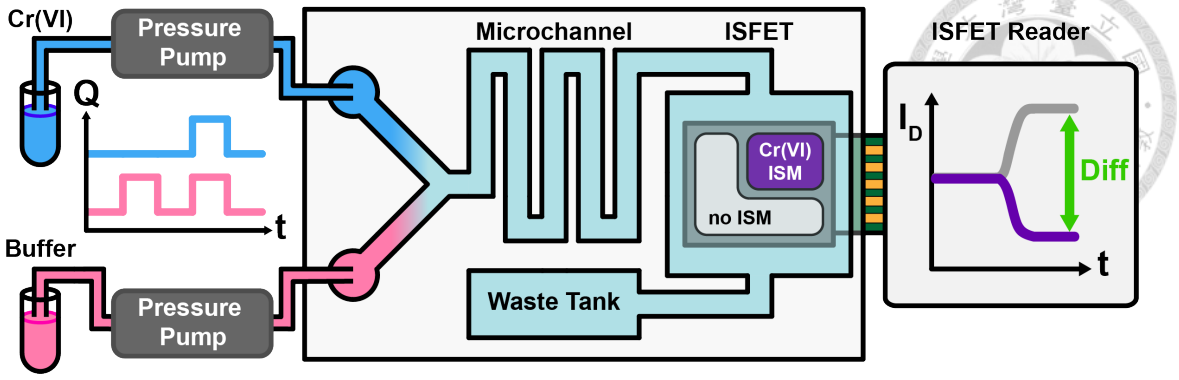

Figure 4-2 ISM-ISFET system integrated pressure pump schematics.

4.2.2 Operation procedures of data processing

From the reader, we could obtain the I_D signal from no ISM area (Sig_{noISM}) and Cr(VI) ISM area (Sig_{CrISM}). First, subtracts each Sig_{CrISM} from Sig_{noISM} we can obtain differential signal ΔI_D ($Sig_{diff} = Sig_{noISM} - Sig_{CrISM}$). Second, the last 20 ΔI_D signals were averaged in each sensing section. Third, the whole ΔI_D signal would be biased where the ΔI_D signal of the first section (usually set as baseline solution measuring with no Cr(VI) contained) was set to zero. Finally, we calculated the averaged value and the standard deviation from the ΔI_D signal of the sample solution.

4.3 ISFET fabrication

The DG-ISFET was fabricated by TSMC [49], as illustrated in Figure 4.3. The top gate material is HfO_2 due to its high dielectric constant, which provides relatively high pH sensitivity and enhanced chemical stability, rendering it suitable for various analytical and biomedical applications [50]. The source, drain, and channel regions on the silicon substrate are defined through ion implantation. Subsequently, a layer of poly-silicon bottom gate is deposited on these regions. Following this step, metal wires are defined and connected to the electrodes and conductive wires. The substrate on the underside is etched away, and a second substrate is flipped and positioned to reveal the original substrate on the top. The embedded oxide layer on the underside is subsequently removed,

doi:10.6342/NTU202401040

and the sensing area is delineated. Finally, HfO_2 is applied to the surface of the chip to act as the dielectric for the top gate. [51].

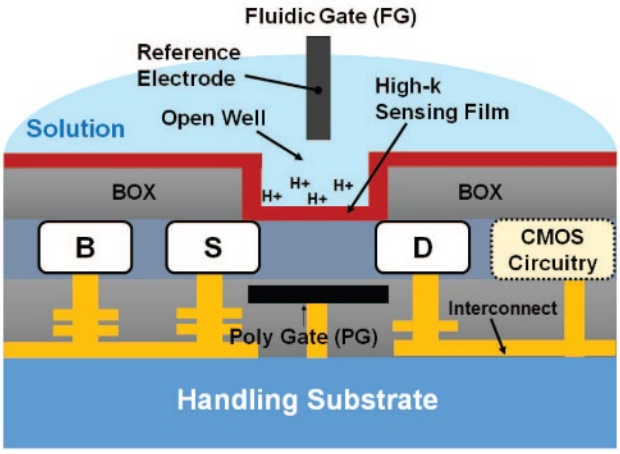

Figure 4-3 Cross-sectional view of DG-ISFET featuring a back-side structure [49].

4.4 PMMA microchannel fabrication

We fabricated the designed pattern with a computer numerical control (CNC) machine (EGX-400, Roland DGA) (Figure 4-4 (A)). Figure 4-4 (B) shows the design of the microchannel with a transparent 3 mm PMMA board. The volume of the microchannel region was 85 μL. The volume of the sensing chamber for Cr(VI) detection was 200 μL. The capacity of the waste tank at the bottom-left region was approximately 2 mL. The inlet and outlet were 2.2 mm diameter holes to match the size of the pressure pump.

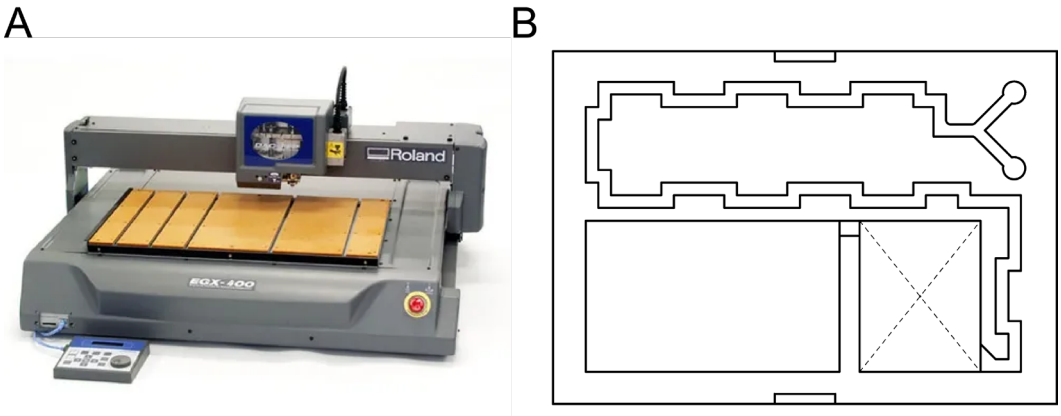

Figure 4-4 (A) Photo of the Roland EGX-400 CNC machine, (B) The schematic of the microchannel.

doi:10.6342/NTU202401040

4.5 ISM solution preparation

The Cr(VI) ISM consists of the following materials [33]:

1. High-molecular-weight poly (vinyl chloride) (PVC): the primary constituent material for porous structured ion-selective membrane.
2. Plasticizer 2-nitro phenyl octyl ether: solidifying and shaping PVC in liquid.
3. Sodium tetra phenyl borate (NaTPB): anion-excluder.
4. Quinaldine red: Cr(VI) specific ionophore.
5. Tetrahydrofuran (THF): easily volatile organic solvents

To prepare the Cr(VI) ISM, 150 mg of plasticizer, 6 mg of NaTPB, and 30 mg of quinaldine red were combined and stirred for 30 min. In the meantime, 114 mg of PVC and 3 mL of THF were mixed and stirred for 30 min. Next, we poured the two solutions together and stirred them overnight to confirm that the cocktail was completely mixed. Finally, the Cr(VI) ISM solutions were stored in a 4℃ refrigerator to prevent solidification. Before the drop-casting procedure, the ISFET will be washed with distilled water (DI) and baked in the 65℃ oven for 10-15 min to ensure no residual liquid is on the ISFET. Also, remove the ISM liquid from the refrigerator and continue stirring for at least five minutes. During the drop-casting, carefully and swiftly withdraw the required amount of ISM liquid, and immediately dispense it onto the surface of the ISFET. Be cautious to avoid air bubbles that might form near the bottom of the tip, as they could potentially adhere to the ISM. After the drop-casting process, the ISM-integrated DG-ISFET was dried for 30 min before detection experiments.

4.6 Standard solution and water sample preparation

Three pH solutions (pH 7, 6, 5; DAEJUNG Corp.), nine $K_2Cr_2O_7$ aqueous solutions (10^{-8}, 10^{-7}, 10^{-6}, $10^{-5.5}$, 10^{-5}, $10^{-4.5}$, 10^{-4}, 10^{-3}, 10^{-2} M) were used for sensor quality and

doi:10.6342/NTU202401040

performance validation. The concentration range of the standard solution was chosen based on the WHO standard of industrial water. (Assisted by Professor Juen-Kai Wang in Academia Sinica). The water samples were collected with a 50 mL centrifuge tube. The sample was collected from the irrigation canal of Sec. 3, Xinsheng S. Rd., Da' an Dist., Taipei City, Taiwan (R.O.C.).

doi:10.6342/NTU202401040

Chapter 5 Results and Discussion

This chapter would be divided into four parts: (1) chip: the ISFET ion sensing performance without any Cr(VI) ISM deposited and the correlation between the volume of ISM solution and the real ISM thickness. (2) Cr(VI) ISM: test the ISM sensitivity and selectivity under different ISM thicknesses to find the best parameter. (3) Buffer: test different concentrations of electrolyte buffer to minimize the interference from the pH value of the sample. (4) Pump-channel system: integrate the pump-channel system and ISM-ISFET to measure the concentration of Cr(VI) automatically.

5.1 Pure ISFET performance

5.1.1 pH and Cr(VI) sensing performance

We prepared three pH solutions (pH value at 7, 6, and 5) and five potassium dichromate solutions ($K_2Cr_2O_7$ = 10^{-6}, $10^{-5.5}$, 10^{-5}, $10^{-4.5}$, 10^{-4} M). Each concentration solution was dropped 200 μL on the sensor for 3 min detection, then rinsed with the next solution twice. The corresponding I_D were recorded simultaneously by the portable reader, and the data processing was shown in Figure 5-1 and Figure 5-2. The last 20 I_D signals were averaged at each sensing section. Then, we calculated the averaged I_D value and the standard deviation, which indicated the sensitivity and stability of the ISFET.

As shown in Figure 5-1, we could see that without the ISM modification, the sensor has a high sensitivity for H^+ ion (17.2 μA/pH), which represents the ability of pH value detection of ISFET. The standard deviation were also small, representing the great stability of the device. Then, we compared the ISFET signals and the pH value of a series of Cr(VI) solutions. As shown in Figure 5-2 (B), the ISFET signals were following the pH value of the solution, but not the concentration of Cr(VI). Therefore, for Cr(VI) ion sensing applications in industrial water sensing, we need to deposit the ISM to increase

doi:10.6342/NTU202401040

the specificity to the target ion and reduce signal interference from other ions in the industrial water.

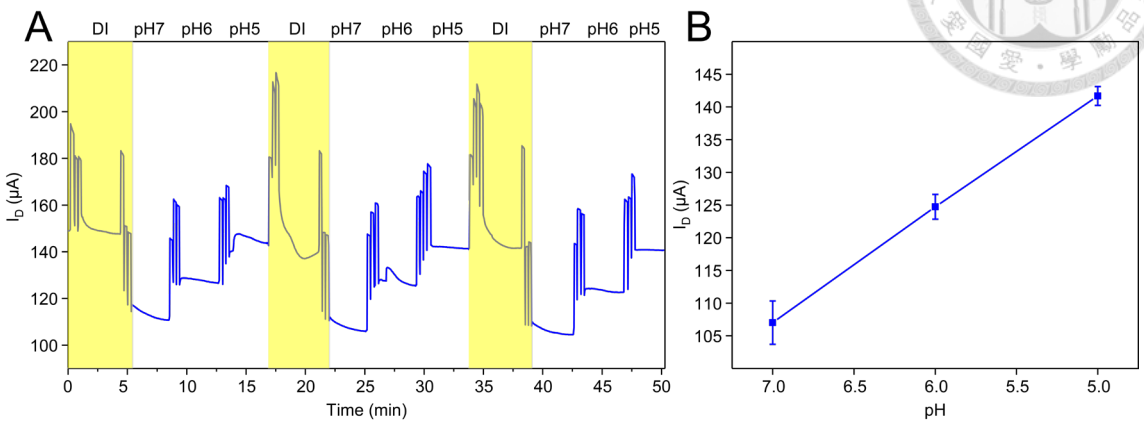

Figure 5-1 (A) The I_D signal with three pH solutions (pH 7, 6, 5), yellow band represents the washing process, (B) Line chart of the average value and standard deviation of each section.

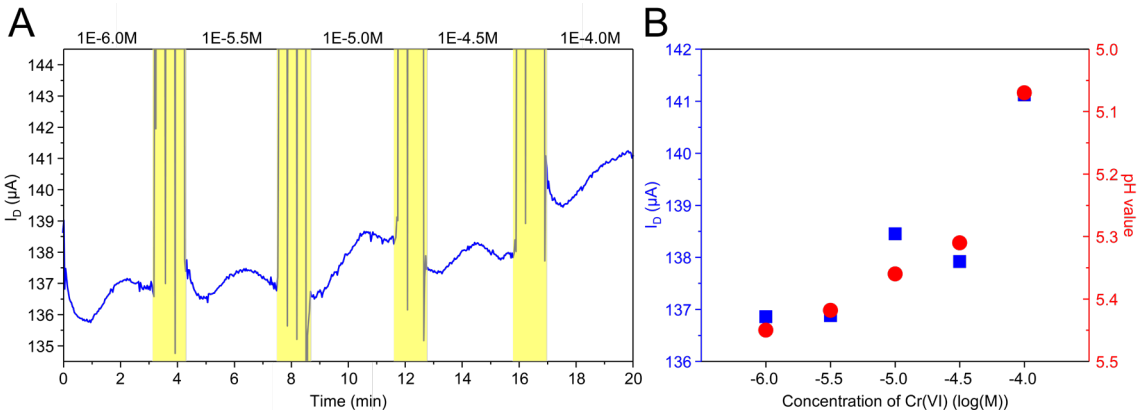

Figure 5-2 (A) The I_D signal with five $K_2Cr_2O_7$ solutions ($10^{-6.0}$, $10^{-5.5}$, $10^{-5.0}$, $10^{-4.5}$, $10^{-4.0}$ M), (B) Scatter chart of the average value of each section (blue dots) and the pH value of corresponding $K_2Cr_2O_7$ solutions (red dots).

5.1.2 Cr(VI) ISM thickness evaluation

Five different volumes (1.5, 2.5, 3.5, 5, 10 μL) of ISM cocktails were deposited into the ISFET by hand to optimize the ISM thickness for the highest sensitivity. To further increase the thickness parameter of the Cr(VI) ISM, we doubled the volume of the

doi:10.6342/NTU202401040

aforementioned ISM liquid and then dropped it onto the chip twice, ensuring consistent surface area while significantly increasing its thickness. A confocal microscopy (Keyence VK-X200 series) with a 10× objective lens measured the average membrane thickness of the ISM with different volumes.

First, as shown in Table 2, we observed that with a thinner thickness, the ISM surface tended to distribute unevenly and generate numerous indentations. This could further affect the standard deviation of different pixels during measurements. In contrast, the thicker ISM exhibits a more uniform distribution, potentially enhancing the stability of the signal. Furthermore, we could see that the thickness slightly increased with a larger volume at the same amount of drops, but significantly increased with the number of drops. Even with the same actual volume (5 × 1 drop and 2.5 × 2 drops), the latter reaches a larger thickness. This is evidently due to the control exerted by the first droplet on the surface area, allowing the ISM to maintain within that range. In contrast, oversized droplets might compress the no ISM area, impacting the stability of the signal in that region.

doi:10.6342/NTU202401040

Table 2 The average thickness of the hand-depositing Cr(VI) ISM measured by the confocal microscopy at ten different volumes.

	Cr(VI) ISM (1 drop)				
volume (μL)	1.5 × 1 drop	2.5 × 1 drop	3.5 × 1 drop	5 × 1 drop	10 × 1 drop
Microscopic images	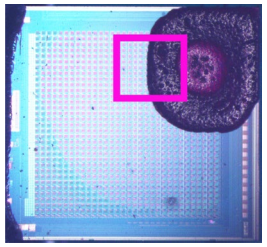	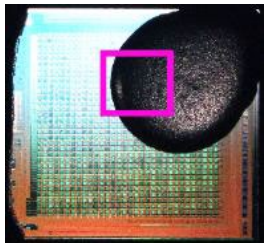	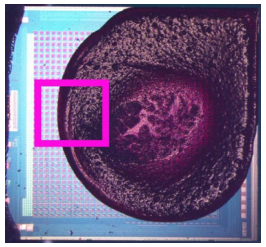	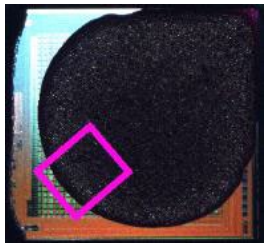	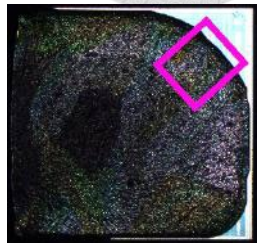
Confocal images	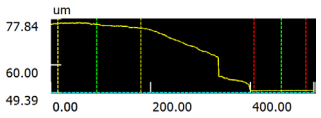	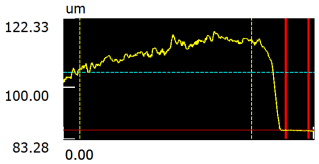	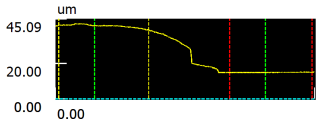	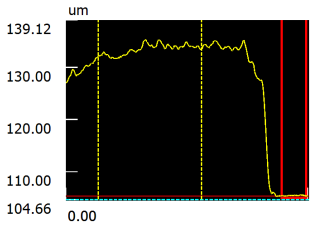	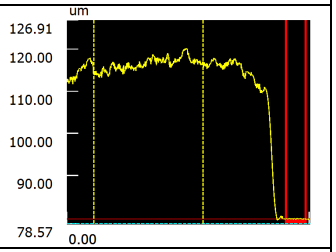
Average thickness (μm)	24.90 (±0.68)	26.62 (±1.97)	26.88 (±1.43)	27.86 (±0.19)	37.02 (±0.81)

doi:10.6342/NTU202401040

	Cr(VI) ISM (2 drops)				
volume (μL)	1.5 × 2 drops	2.5 × 2 drops	3.5 × 2 drops	5 × 2 drops	10 × 2 drops
Microscopic images	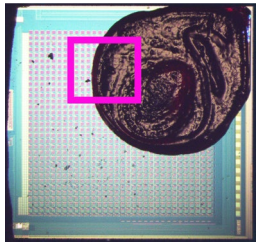	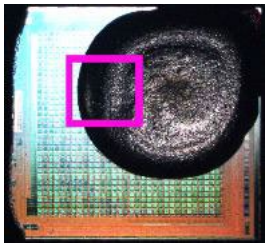	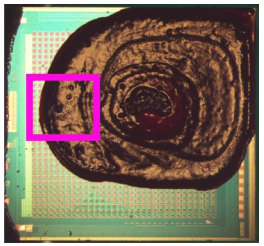	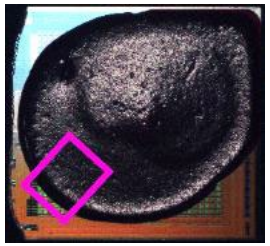	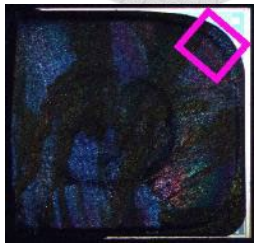
Confocal images	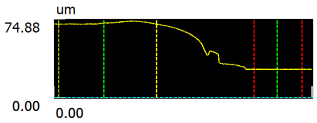	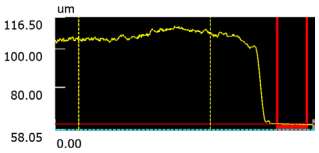	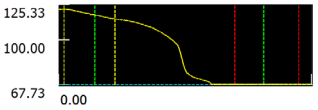	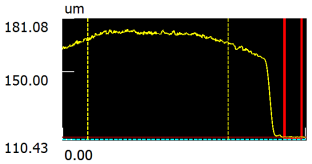	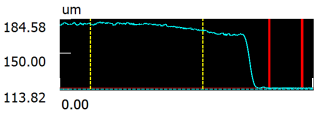
Average thickness (μm)	44.46 (±0.74)	47.34 (±0.69)	48.37 (±1.87)	59.59 (±1.14)	63.35 (±0.46)

doi:10.6342/NTU202401040

5.2 Cr(VI) ISM-ISFET performance

5.2.1 Cr(VI) ISM thickness optimization

After measuring the ISM thickness, we decided to choose six of them for further research: 24.9 μm (1.5 μL), 26.6 μm (2.5 μL), 26.8 μm (3.5 μL), 44.4 μm (1.5×2 μL), 47.3 μm (2.5×2 μL) and 48.4 μm (3.5×2 μL). All of them have a small enough ISM surface area, leaving enough space for non-ISM sensing. As shown in Figure 5-3, we measured the continuous I_D current and corresponding differential signal ΔI_D (A-G) under No ISM and six different thicknesses of ISM using DI water solution and six $K_2Cr_2O_7$ solution (10^{-8}, 10^{-7}, 10^{-6}, 10^{-5}, 10^{-4}, and 10^{-3} M) to test the sensitivity.

First, the performance of Cr(VI) ISM is significant; the signals increase with the increase of Cr(VI). we could also confirm that differential sensing shows great performance at eliminating the noise of the original signal through Figure 5-3 (A-G), the differential signal ΔI_D showed a stable response to the concentration of Cr(VI) while having dissimilar original signals in different experiments.

Next, we could observe the relationship between the thickness of ISM and the duration of measurement. As shown in Figure 5-3, when the ISM thickness is thinner (less volume of ISM liquid), the signal is more easily stabilized, but the standard deviation is relatively larger. This is because the thinner ISM surface is more prone to unevenness, leading to greater signal differences between different pixels. In contrast, thicker ISM requires more time to stabilize the signal, but the standard deviation is much smaller. The only exception is the ISM of 48.4 μm (3.5×2 μL), which despite having high sensitivity, also exhibited a very large standard deviation. This is likely due to the excessive thickness, resulting in a prolonged time required for signal stabilization. As a result, within the fixed measurement interval, different pixels could not obtain consistent signals.

doi:10.6342/NTU202401040

According to Figure 5-3 (H), we observe the signals rebound when reaching lower concentrations (10^{-7} and 10^{-8} M), which could lead to misreading when measuring a sample solution with an unknown concentration of Cr(VI). This phenomenon was more pronounced with thinner ISM which both 10^{-7} and 10^{-8} M exhibited signal rebound, whereas with thicker ISM, signal rebound occurred only at 10^{-8} M.

Based on the discussions above, ISM of 47.3 μm (2.5×2 μL) has an excellent sensitivity of 1.3 / 3.3 / 8.0 (μA / log(M)) since 10^{-6} M. Also, considering its minimal standard deviation and the smallest signal rebound, it was chosen for further experiments.

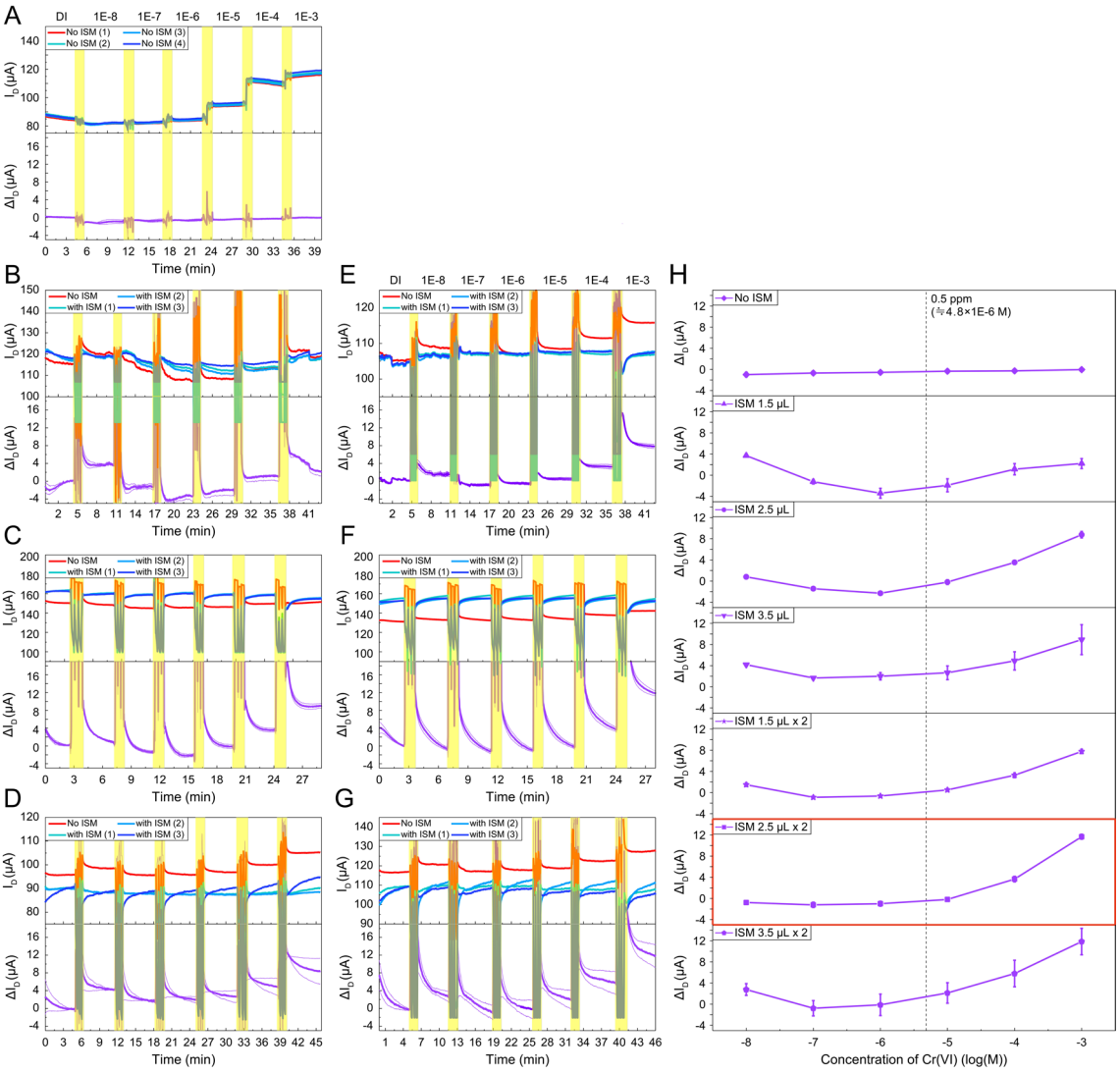

Figure 5-3 (A-G) The I_D and ΔI_D signal of DI water solution and $K_2Cr_2O_7$ solution (10^{-8}, 10^{-7}, 10^{-6}, 10^{-5}, 10^{-4}, 10^{-3} M) with (A) no ISM; ISM of (B) 24.9 μm (1.5 μL); (C) 26.6

doi:10.6342/NTU202401040

μm (2.5 μL); (D) 26.8 μm (3.5 μL); (E) 44.4 μm (1.5×2 μL); (F) 47.3 μm (2.5×2 μL); (G) 48.4 μm (3.5×2 μL), (H) Average value and standard deviation of corresponding signal. The vertical dash line represents the WHO standard of Cr(VI) in wastewater.

5.2.2 PBS buffer solution concentration optimization

The signal rebound problem might have two reasons under low concentration of Cr(VI) and electrolyte solution: First, its pH value was higher than pH 5.6 – 5.7, which might cause the transition of Cr(VI) aqueous form from $Cr_2O_7^{2-}$ to CrO_4^{2-}, weaken the affinity of ionophore. Second, low electrolyte concentration would amplify the specificity of ISFET towards H^+ ions. Also, it would lead to a low concentration gradient, making the concentration balance across the Cr(VI) ISM much harder. These reasons would eventually compress the Cr(VI) signal and amplify the signal given by the pH difference across the ISM.

To improve the signal rebound problem further, we prepared a standard solution mixed with a specific concentration of electrolytes using PBS buffer solution. First, we measured the pH value of six $K_2Cr_2O_7$ solutions (10^{-8}, 10^{-7}, 10^{-6}, 10^{-5}, 10^{-4}, 10^{-3} M) in DI water, and in four different PBS buffer solutions (10^{-7}, 10^{-6}, 10^{-5}, 10^{-4} M). According to Figure 5-4 (A), the pH value of Cr(VI) in low concentration would be significantly influenced by the pH value of its PBS buffer solution, which proved that PBS could control the pH value to a certain range in low Cr(VI) concentration, to stabilize the Cr(VI) aqueous form and minimize the H^+ ions difference in different Cr(VI) concentration.

Then, we measured a series of Cr(VI) concentrations in four different PBS buffer solutions through ISM-ISFET. Considering the importance of distinguishing signals around the WHO standard of Cr(VI), we measured six $K_2Cr_2O_7$ (10^{-8}, 10^{-7}, 10^{-6}, 10^{-5}, 10^{-4}, 10^{-3} M) in four different PBS buffer solution (10^{-7}, 10^{-6}, 10^{-5}, 10^{-4} M) with ISM of 47.3

doi:10.6342/NTU202401040

μm. As shown in Figure 5-4 (B), the signal rebound decreases and sensitivity increases as the concentration of PBS becomes higher in the range of 10^{-7}, 10^{-6}, and 10^{-5} M. On the other hand, PBS 10^{-4} M shows the lowest signal rebound but worst sensitivity during measurement, only having the highest signal at Cr(VI) 10^{-3} M. This is due to the high average pH value of Cr(VI) solution in PBS 10^{-4} M, leading to the conversion of Cr(VI) into other forms, thereby reducing its affinity with the ionophore. Based on these results, a PBS buffer solution of 10^{-5} M has been chosen for further experiments.

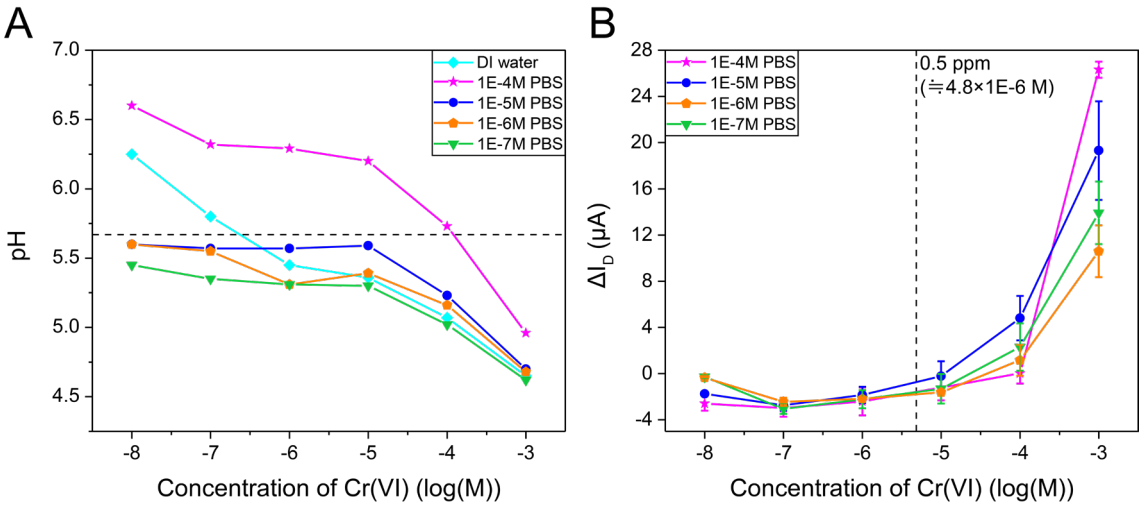

Figure 5-4 (A) pH value of different concentration of Cr(VI) in DI water, and in four different PBS buffer solution (10^{-7}, 10^{-6}, 10^{-5}, 10^{-4} M), the dash line represents pH 5.67, (B) Differential signal ΔI_D of $K_2Cr_2O_7$ solution (10^{-8}, 10^{-7}, 10^{-6}, 10^{-5}, 10^{-4}, 10^{-3} M) in four different PBS buffer solution (10^{-7}, 10^{-6}, 10^{-5}, 10^{-4} M) with ISM of 47.3 μm.

5.2.3 Sensitivity and Selectivity of Cr(VI) ISM-ISFET

We measured the sensitivity of ISM-ISFET with eight $K_2Cr_2O_7$ solutions (10^{-8}, 10^{-7}, 10^{-6}, $10^{-5.5}$, 10^{-5}, $10^{-4.5}$, 10^{-4}, 10^{-3} M) in PBS buffer solution of 10^{-5} M with ISM of 47.3 μm. As shown by the blue line in Figure 5-5 (A), the ISM-ISFET showed great sensitivity from Cr(VI) 10^{-7} to 10^{-3} M while having excellent stability during measurement. Comparing Figure 5-3 (H) to Figure 5-5 (A), an ISM of 47.3 μm showed a greater signal

doi:10.6342/NTU202401040

both at low and high Cr(VI) concentrations. The former results confirmed that increasing the concentration of electrolytes helps inhibit the signal rebound. The latter performance might be due to the increase of ionic strength, which would lead to a decrease in ISM resistivity, thus changing the activities of analyte ion in the ISM and increasing the Donnan potential (Equation(18)), finally increasing the signal. As shown in Figure 5-5 (B), the calibration curve has a linear range from 10^{-6} M to $10^{-4.5}$ M, and the slope was 2.05 μA / log(M) with an R-square of 0.963. These results proved that this device can precisely measure the Cr(VI) concentration near the WHO standard, showing great sensitivity and stability, thus having great potential for industrial water sensing.

To measure the selectivity of ISM, we prepared a bunch of heavy metal ions (Zn(II), Fe(II), Cu(II), Cr(III)) for the selectivity test. All of the tested ions were prepared at a concentration of 5×10^{-4} M, which is much higher (100×) than their WHO standard. We measured the differential signal ΔI_D with no ISM (Figure 5-5 (C)) and with ISM 47.3 μm (Figure 5-5 (D)). In Figure 5-5 (C), the signal distribution is very close to the pH value of the tested ion solutions without ISM, showing the normal performance of ISFET. As shown in Figure 5-5 (D), the Cr(VI) signal has a much higher signal through differential sensing compared to any other tested ions, even Cr(III). This result shows that Cr(VI) ISM can distinguish between Cr(III) and Cr(VI), which is an important indicator for the Cr(VI) sensor.

doi:10.6342/NTU202401040

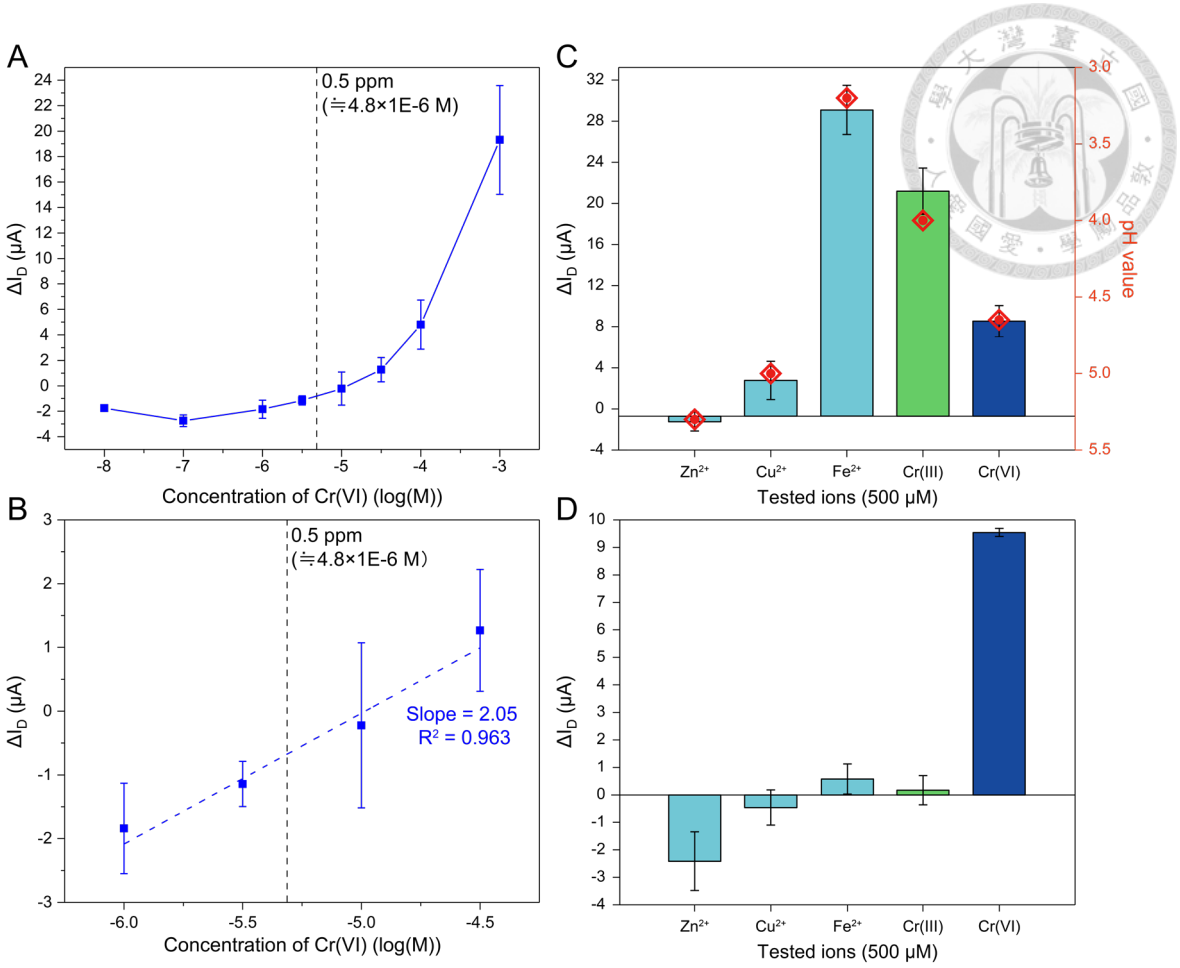

Figure 5-5 (A) Average value and standard deviation of eight $K_2Cr_2O_7$ solutions (10^{-8}, 10^{-7}, 10^{-6}, $10^{-5.5}$, 10^{-5}, $10^{-4.5}$, 10^{-4}, 10^{-3} M) in 10^{-5} M PBS buffer solution with ISM of 47.3 μm, (B) analysis of linear regression of the signals between 10^{-6} M to $10^{-4.5}$ M, R-square is 0.963, slope is 2.05 μA / log(M), (C-D) differential signal ΔI_D of different tested ions (5×10^{-4} M) including Zn(II), Fe(II), Cu(II), Cr(III) and Cr(VI) with (C) No ISM; (D) ISM 47.3 μm. Red dots represent the pH value of the corresponding tested ion solutions.

5.2.4 Cr(VI) sensing in ditch water using the Cr(VI) ISM-ISFET

At the end of the ISM-ISFET off-channel test, we measured the performance of the sample solution with a ditch water background. We obtained the ditch water and spiked it in a series of known Cr(VI) concentrations with 10^{-5} M PBS buffer solution; the ditch water would be diluted to half during the procedure. We measured both a wide range (from 10^{-8} to 10^{-3} M) and a relatively small Cr(VI) range (from 10^{-6} to 10^{-4} M) close to

doi:10.6342/NTU202401040

the WHO standard concentration. The results were shown in Figure 5-6 (A-B); ISM-ISFET showed extremely excellent performance in ditch water background, proving that Cr(VI) ISM can separate the Cr(VI) signal with other interference ions signal by differential sensing while having great stability, which is confirmed by the signals close to the calibration curve in Figure 5-6 (C). The signal rebound problem was successfully inhibited, too, though the signal could hardly be distinguished under a concentration of 10^{-6} M; all of the signals were under the dashed line of the WHO standard signal, showing great performance in measuring the concentration of Cr(VI) in the sample exceeded the WHO standard or not. Figure 5-6 (D) compared the linear regression analysis between measurements in the DI background and ditch water background. The device in the ditch water showed almost the same R-square, while the slope was slightly greater than the calibration curve, showing the perfect stability of the ISM and the ISFET.

doi:10.6342/NTU202401040

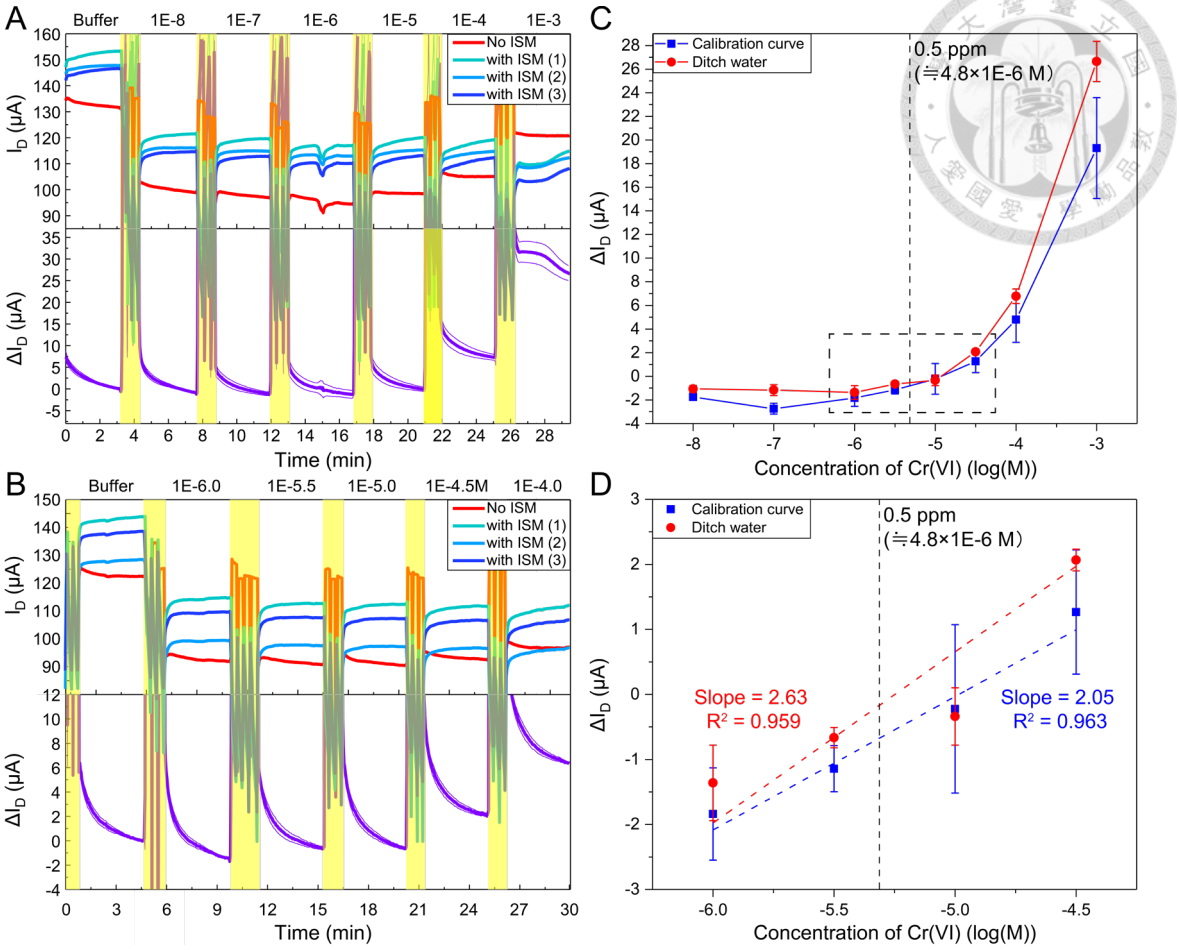

Figure 5-6 (A-B) The I_D and ΔI_D signal of 10^{-5} M PBS buffer and $K_2Cr_2O_7$ solution (A) in wide Cr(VI) range (10^{-8}, 10^{-7}, 10^{-6}, 10^{-5}, 10^{-4}, 10^{-3} M); (B) in small Cr(VI) range ($10^{-6.0}$, $10^{-5.5}$, $10^{-5.0}$, $10^{-4.5}$, $10^{-4.0}$ M) with 10^{-5} M PBS buffer in ditch water background with ISM of 47.3 μm, (C) Average value and standard deviation of both signals compared with a calibration curve of ISM 47.3 μm (Figure 5-5 (A)), (D) Linear regression analysis of signals in (C) in the range of $10^{-6.0}$ M to $10^{-4.5}$ M.

5.3 Pump-channel system performance

5.3.1 pH sensing in DI water using the pump-channel system

To exclude the potential issue of the pump-channel system for further measurement, we first measured three pH solutions (pH value at 7, 6, and 5) back and forth to test the performance and stability of ISFET in this environment. As shown in Figure 5-7, the

doi:10.6342/NTU202401040

signal of the same solution at different measuring times remained the same, while the whole noise became fuzzier than when measuring off-channel. This might be due to the unexpected flow of sample solution in the channel since it was not airtight while the pumps were closed. We used a dovetail clip to clamp the Tygon tube for a solution. Despite the issue, ISFET still shows great performance for pH standard solution sensing.

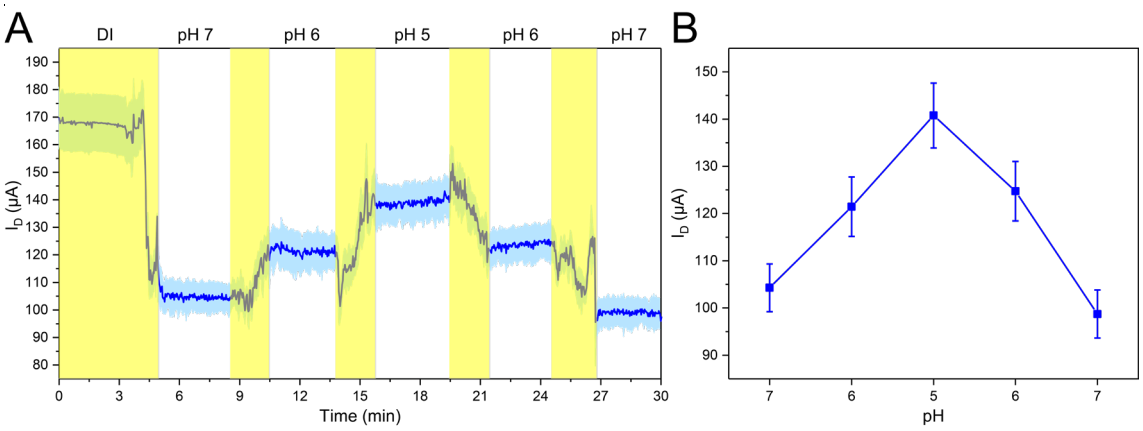

Figure 5-7 (A) The I_D signal with five pH solutions (pH 7, 6, 5, 6, 7) measured by ISFET with no ISM using the pump-channel system, (B) Line chart of the average value and standard deviation of each section.

5.3.2 Cr(VI) sensing in DI water using the pump-channel system

Once confirmed the function of the pump-channel system, we mixed both the Cr(VI) series in wide range (from 10^{-8} to 10^{-3} M) and small range (from 10^{-6} to 10^{-4} M) with 10^{-5} M PBS buffer in DI water background in 1:1 scale using microchannel, measured using ISM-ISFET under ISM thickness of 47.3 μm, and compared the results to the calibration curve of ISM 47.3 μm in Figure 5-5 (A). Considering the sample solution would be diluted 2 times, we prepared the sample solution in double concentration. As shown in Figure 5-8, although the original signal seems fuzzy with an unexpected pulse, the differential signals were still very close to the calibration curve (Figure 5-8 (C)), showing great performance with the integration of the pump-channel system. The linear regression

doi:10.6342/NTU202401040

analysis in Figure 5-8 (D) revealed the R-square decrease from 0.963 to 0.798. The main reason was the signal offset happened at $10^{-5.5}$ M, which may be improved by solving the airtight issue of pressure pumps.

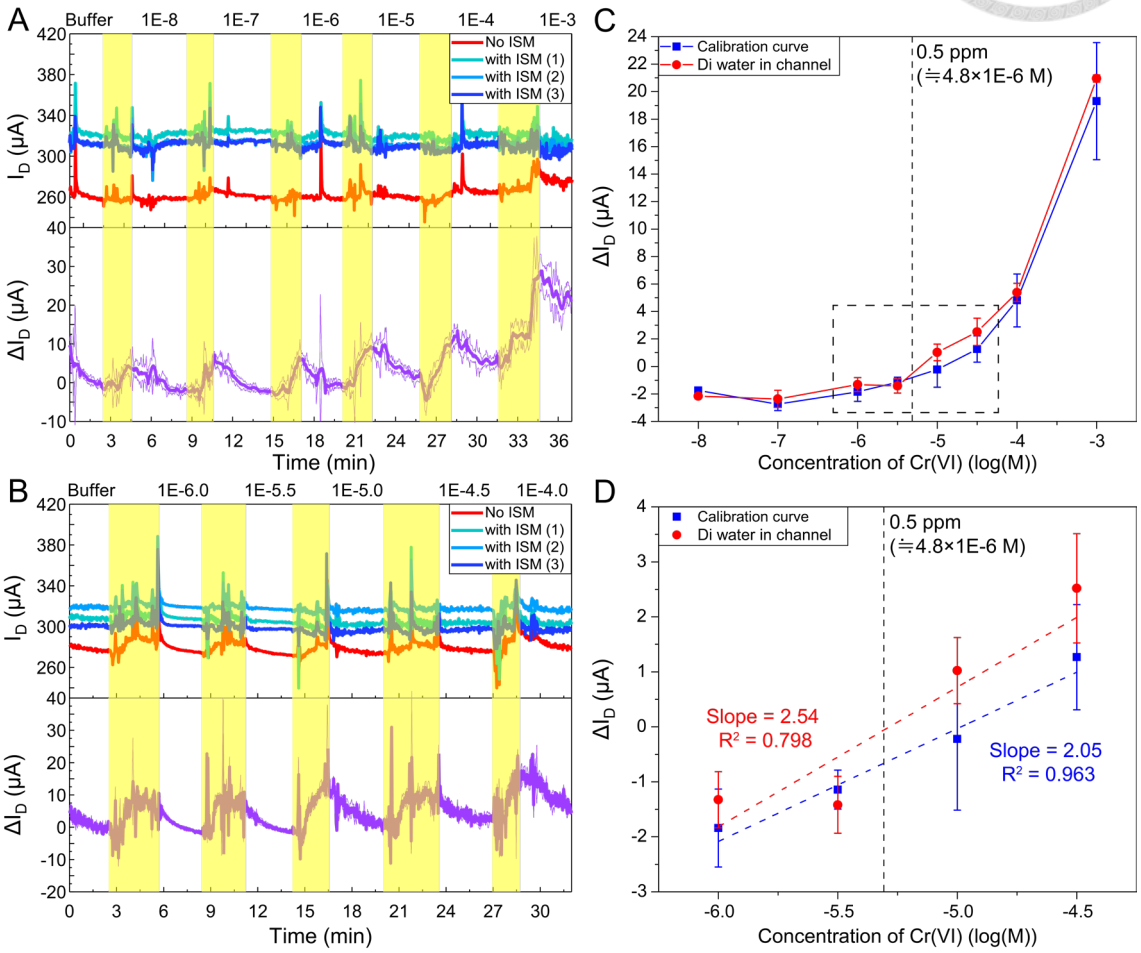

Figure 5-8 (A-B) The I_D and ΔI_D signal of 10^{-5} M PBS buffer and $K_2Cr_2O_7$ solution (A) in wide Cr(VI) range (10^{-8}, 10^{-7}, 10^{-6}, 10^{-5}, 10^{-4}, 10^{-3} M); (B) in small Cr(VI) range ($10^{-6.0}$, $10^{-5.5}$, $10^{-5.0}$, $10^{-4.5}$, $10^{-4.0}$ M) with 10^{-5} M PBS buffer in DI water background with ISM of 47.3 μm using pump-channel system, (C) Average value and standard deviation of both signals compared to calibration curve of ISM 47.3 μm (Figure 5-5 (A)), (D) Linear regression analysis of signals in (C) in the range of $10^{-6.0}$ M to $10^{-4.5}$ M.

5.3.3 Cr(VI) sensing in ditch water using the pump-channel system

Finally, we measured a series of $K_2Cr_2O_7$ solutions mixed with 10^{-5} M PBS in a ditch

doi:10.6342/NTU202401040

water background using a microchannel. As shown in Figure 5-9 (A-B), one could observe that the signal became less fuzzy than when pH was measured. This might be due to the relatively strong ionic strength given by the ditch water background. Also, comparing the difference between DI and ditch water background, the latter shows much lower I_D signals and represents a higher pH value than the DI background. This might decline the pH value control ability of PBS buffer, causing a signal rebound in the low concentration of Cr(VI). Also, from Figure 5-9 (A) we could observe that the original signal where still decreasing at the end of the 10^{-8} M section, representing that the signal rebound might happened because of the insufficient reaction time of the pump-channel system integrated ISFET in ditch water background, which could be further improved. Despite that, as shown in Figure 5-9 (D), the linear regression analysis showed the great performance of the system. The slope is 2.24 while the R-square is 0.943, which is very close to the calibration curve. Overall, ISM-ISFET showed great performance for Cr(VI) sensing. In Figure 5-9 (C-D), we could still observe the ability to distinguish exceeded signal and non-exceeded signal down to 10^{-6} M. Therefore, we proved this system could perform on-site Cr(VI) ion detection in water automatically.

doi:10.6342/NTU202401040

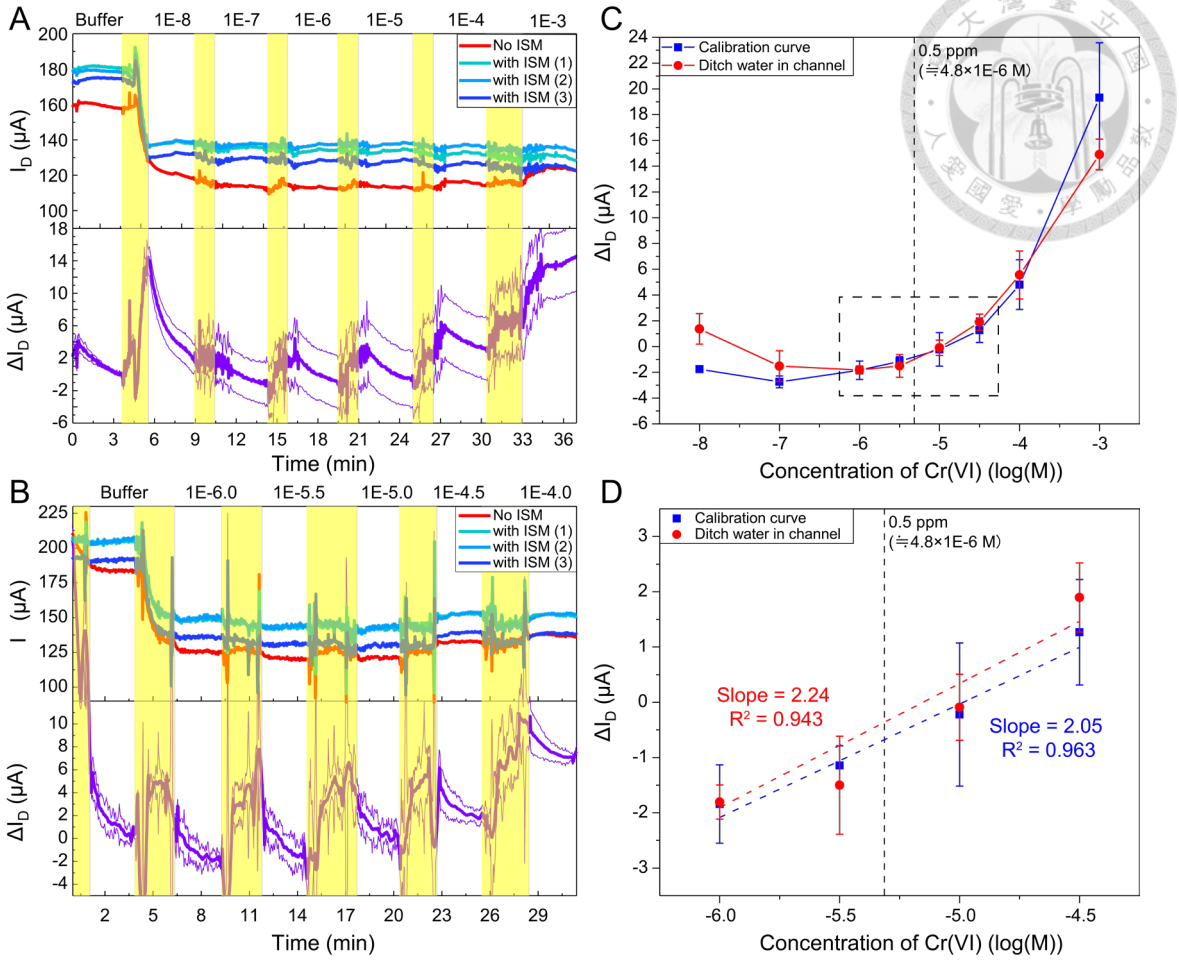

Figure 5-9 (A-B) The I_D and ΔI_D signal of 10^{-5} M PBS buffer and $K_2Cr_2O_7$ solution (A) in wide Cr(VI) range (10^{-8}, 10^{-7}, 10^{-6}, 10^{-5}, 10^{-4}, 10^{-3} M); (B) in small Cr(VI) range ($10^{-6.0}$, $10^{-5.5}$, $10^{-5.0}$, $10^{-4.5}$, $10^{-4.0}$ M) with 10^{-5} M PBS buffer in ditch water background with ISM of 47.3 μm using pump-channel system, (C) Average value and standard deviation of both signals compared to calibration curve of ISM 47.3 μm (Figure 5-5 (A)), (D) Linear regression analysis of signals in (C) in the range of $10^{-6.0}$ M to $10^{-4.5}$ M.

doi:10.6342/NTU202401040

Chapter 6 Conclusion

This research utilized the integration of ISM and ISFET combined with a portable pump-channel system for automatic and in situ Cr(VI) sensing in wastewater samples within 10 min. This platform addresses problems in traditional methods, such as complicated operation processes and large, non-portable instruments. Briefly, there are four important features. First, the differential sensing using Cr(VI) ISM could eliminate the signal interference suffered from drifting issues, pH, and other ions, leaving only the Cr(VI) signal and improving the sensitivity and selectivity. Second, the ISM thickness was optimized at 47.3 μm, with the enhanced signal of 10^{-3} M Cr(VI) from 0.08 to 11.7 μA. Third, to inhibit the signal rebound that occurs at low concentrations of Cr(VI), we optimized the PBS buffer condition at 10^{-5} M to maintain the pH valve and improve the limit of detection of Cr(VI) down to 10^{-7} M, which the signal was improved from -1.03 μA to -2.78 μA. Besides, the signal of 10^{-3} M Cr(VI) was further enhanced from 11.7 μA to 19.3 μA due to the increase in ionic strength. Fourth, the pump-channel system was designed for drawing the sample solution, mixing it with the buffer solution, and guiding the mixing sample into the sensing area automatically. The flow rate of the pump and duration time of each section have been adjusted by Python and operated through a Raspberry Pi computer. In summary, we integrated the pump-channel system with Cr(VI) ISM-embedded ISFET devices to simplify the device and improve the operation time, sensitivity, and selectivity of Cr(VI) ions, which enables in situ ion concentration sensing in wastewater within 10 min.

doi:10.6342/NTU202401040

Chapter 7 Future Work

7.1 ISM fabrication process standardization

The research measured the ISM thickness under different volumes of ISM cocktails. However, these hand-made processes were not stable and uniform, which may cause the lower signal consistency of ISM-ISFET compared with pure ISFET. Furthermore, few researchers discussed the correlation between the ISM-ISFET performance and the width between ISM and ISFET. These parameters may further improve the performance of the device in certain conditions. We could improve the Cr(VI) ISM fabrication process by applying advanced technologies such as deposition, spin coating, and inkjet printing [52], which could standardize the ISM-ISFET manufacturing process and eliminate the variation between the replications of ISMs.

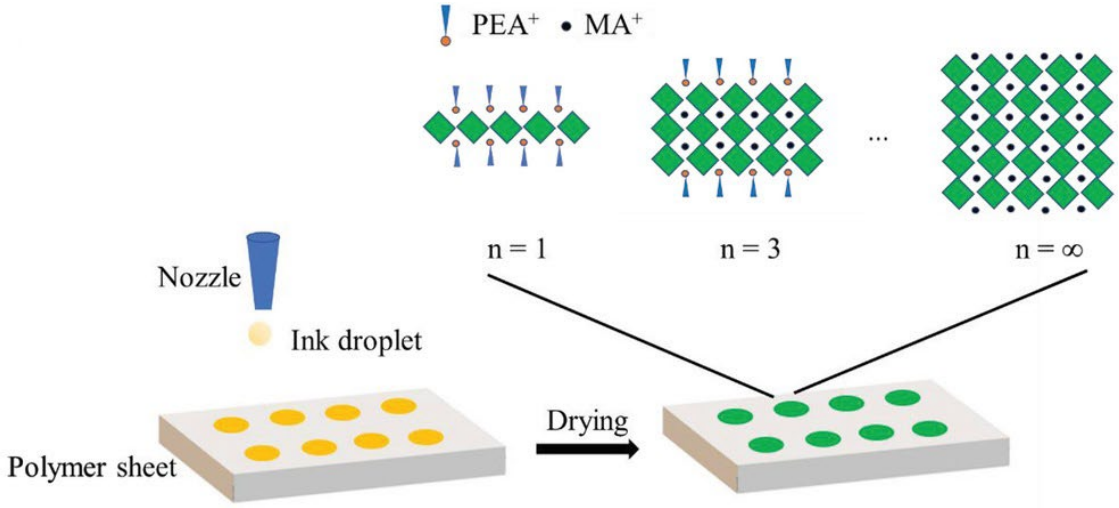

Figure 7-1 (a) Schematic representation of the procedure of inkjet printing [52].

7.2 ISM Reusability and regeneration

The blocking ability of Cr(VI) ISM was accomplished by the interaction of Cr(VI) anions and Quinaldine red. Although it has a relatively high affinity to Cr(VI) anions, it is a challenge to break the connection of these two compounds and refresh the blocking

doi:10.6342/NTU202401040

efficiency of ISM. The total amount of ionophore was sufficient for the whole detection in every experiment in this research, but it would suffer the problem when reaching long duration time measurement. An easy way to avoid the ISM efficiency problem is to change the ISM regularly. However, developing a regeneration process and combine with the standard ISM-ISFET fabrication process mentioned in the previous section would be a more reliable method. A research team reported that a Cr(VI) removal process using highly surface-activated carbon with adsorbent recycling [53] could become a good example for further research. The integration with microfluidic channels is also a great advantage for loading the required solution easily.

7.3 Multiple heavy metal ions sensing

Unlike Cr(VI) anions having complex forms in aqueous solutions, other heavy metal ions remaining in single ions in water have a simpler interaction with their ionophore. In this way, we could deposit multiple heavy metal ionized ISMs on the ISFET array and choose the pixel right under each ISM for simultaneous multiple sensing. The ionophore of Hg(II), Cu(II), and Pb(II) has been developed already; we want to apply other ion carriers to monitor ion concentration more comprehensively and broaden the application of the ISM-ISFET sensor. However, there were already multiple ISMs modified ISFET research [51] that observed the cross-influence to the performance of each membrane; there would still be a challenge for developing multiple ISM sensing while maintaining the sensitivity and selectivity of each ISM performance.

doi:10.6342/NTU202401040

REFERENCES

[1] J. Zhang, and S. Li, "Sensors for detection of Cr(VI) in water: a review," *International Journal of Environmental Analytical Chemistry,* vol. 101, no. 8, pp. 1051-1073, 2021/06/21, 2021.

[2] N. Joseph, and B. Manoj, "Nanomaterials-Based Chemical Sensing," *Nanotechnology for Electronic Applications*, N. M. Mubarak, S. Gopi and P. Balakrishnan, eds., pp. 131-147, Singapore: Springer Nature Singapore, 2022.

[3] R. K. Tandon, P. T. Crisp, J. Ellis, and R. S. Baker, "Effect of pH on chromium(VI) species in solution," *Talanta,* vol. 31, no. 3, pp. 227-228, 1984/03/01/, 1984.

[4] K. H. Cheung, and J.-D. Gu, "Mechanism of hexavalent chromium detoxification by microorganisms and bioremediation application potential: A review," *International Biodeterioration & Biodegradation,* vol. 59, no. 1, pp. 8-15, 2007/01/01/, 2007.

[5] M. A. Zaitoun, "Spectrophotometric determination of Chromium(VI) using cyclam as a reagent," *International Journal of Environmental Analytical Chemistry,* vol. 85, no. 6, pp. 399-407, 2005/05/15, 2005.

[6] A. N. Anthemidis, G. A. Zachariadis, and J. A. Stratis, "On-line preconcentration and determination of copper, lead, and chromium(VI) using unloaded polyurethane foam packed column by flame atomic absorption spectrometry in natural waters and biological samples," *Talanta,* vol. 58, no. 5, pp. 831-840, 2002/11/12/, 2002.

[7] T. Braun, and A. B. Farag, "Polyurethane foams and microspheres in analytical chemistry: Improved liquid-solid, gas-solid and liquid-liquid contact via a new geometry of the solid phase," *Analytica Chimica Acta,* vol. 99, no. 1, pp. 1-36, 1978/07/01/, 1978.

[8] M. Ezoddin, F. Shemirani, and R. Khani, "Application of mixed-micelle cloud point extraction for speciation analysis of chromium in water samples by electrothermal atomic absorption spectrometry," *Desalination,* vol. 262, no. 1, pp. 183-187, 2010/11/15/, 2010.

[9] M. Noroozifar, and M. Khorasani-Motlagh, "Specific Extraction of Chromium as Tetrabutylammonium-Chromate and Spectrophotometric Determination by Diphenylcarbazide: Speciation of Chromium in Effluent Streams," *Analytical Sciences,* vol. 19, no. 5, pp. 705-708, 2003/05/01, 2003.

[10] D. G. Themelis, F. S. Kika, and A. Economou, "Flow injection direct spectrophotometric assay for the speciation of trace chromium(III) and chromium(VI) using chromotropic acid as chromogenic reagent," *Talanta,* vol. 69, no. 3, pp. 615-620, 2006/05/15/, 2006.

[11] Z. Zhao, R. Gao, J. Li, S. Liu, and H. Liu, "Chromotropic Acid as a Reagent for Ultraviolet Spectrophotometric Determination of Hexavalent Chromium in Water," *Microchemical Journal,* vol. 58, no. 1, pp. 1-5, 1998/01/01/, 1998.

[12] J. Guertin, J. A. Jacobs, and C. P. Avakian, *Chromium (VI) handbook*: CRC press, 2004.

[13] L. A. Malik, A. Bashir, A. Qureashi, and A. H. Pandith, "Detection and removal of heavy metal ions: a review," *Environmental Chemistry Letters,* vol. 17, no. 4, pp. 1495-1521, 2019/12/01, 2019.

[14] S. Babazadeh, R. Bisauriya, M. Carbone, L. Roselli, D. Cecchetti, E. M. Bauer, S. Sennato, P. Prosposito, and R. Pizzoferrato, "Colorimetric Detection of

doi:10.6342/NTU202401040

Chromium(VI) Ions in Water Using Unfolded-Fullerene Carbon Nanoparticles," *Sensors (Basel),* vol. 21, no. 19, Sep 23, 2021.
[15] N. N. Nghia, B. T. Huy, and Y.-I. Lee, "Colorimetric detection of chromium(VI) using graphene oxide nanoparticles acting as a peroxidase mimetic catalyst and 8-hydroxyquinoline as an inhibitor," *Microchimica Acta,* vol. 186, no. 1, pp. 36, 2018/12/18, 2018.
[16] P. Joshi, S. Sarkar, S. K. Soni, and D. Kumar, "Label-free colorimetric detection of Cr(VI) in aqueous systems based on flower shaped silver nanoparticles," *Polyhedron,* vol. 120, pp. 142-149, 2016/12/14/, 2016.
[17] K. J. Lee, N. Elgrishi, B. Kandemir, and J. L. Dempsey, "Electrochemical and spectroscopic methods for evaluating molecular electrocatalysts," *Nature Reviews Chemistry,* vol. 1, no. 5, pp. 0039, 2017/05/10, 2017.
[18] A. K. Jain, V. K. Gupta, L. P. Singh, P. Srivastava, and J. R. Raisoni, "Anion recognition through novel C-thiophenecalix[4]resorcinarene: PVC based sensor for chromate ions," *Talanta,* vol. 65, no. 3, pp. 716-721, 2005/02/15/, 2005.
[19] B. Dalkıran, H. E. Kormalı Ertürün, A. D. Özel, E. Canel, S. Özkınalı, and E. Kılıç, "Chromate-selective electrodes prepared by using calix[4]arenes for the speciation of Cr(VI) and Cr(III)," *Ionics,* vol. 23, no. 9, pp. 2509-2519, 2017/09/01, 2017.
[20] Y.-W. Choi, N. Minoura, and S.-H. Moon, "Potentiometric Cr(VI) selective electrode based on novel ionophore-immobilized PVC membranes," *Talanta,* vol. 66, no. 5, pp. 1254-1263, 2005/06/15/, 2005.
[21] M. R. Ganjali, M. H. Eshraghi, S. Ghadimi, and S. Mojtaba, "Novel chromate sensor based on MWCNTs/Nanosilica/Ionic Liouid/Eu complex/graphite as a new nano-composite and its application for determination of chromate ion concentration in waste water of chromium electroplating," *Int. J. Electrochem. Sci,* vol. 6, pp. 739-748, 2011.
[22] M. Rezayi, M. Ghasemi, R. Karazhian, M. Sookhakian, and Y. Alias, "Potentiometric Chromate Anion Detection Based on Co(SALEN)2 Ionophore in a PVC-Membrane Sensor," *Journal of The Electrochemical Society,* vol. 161, no. 6, pp. B129, 2014/04/30, 2014.
[23] A. Benvidi, M. Elahizadeh, H. R. Zare, and R. Vafazadeh, "Highly Sensitive Membrane Electrode Based on a Copper(II)-bis(N-4-Methylphenyl-Salicyldenaminato) Complex for the Determination of Chromate," *Analytical Letters,* vol. 44, no. 4, pp. 595-606, 2011/02/15, 2011.
[24] M. M. Ardakani, A. Dastanpour, and M. Salavati-Niasari, "Novel Coated-Wire Membrane Sensor Based on Bis(Acetylacetonato) Cadmium(II) for the Determination of Chromate Ions," *Microchimica Acta,* vol. 150, no. 1, pp. 67-72, 2005/05/01, 2005.
[25] I. Švancara, K. Vytřas, K. Kalcher, A. Walcarius, and J. Wang, "Carbon Paste Electrodes in Facts, Numbers, and Notes: A Review on the Occasion of the 50-Years Jubilee of Carbon Paste in Electrochemistry and Electroanalysis," *Electroanalysis,* vol. 21, no. 1, pp. 7-28, 2009.
[26] H. Ju, S. Liu, B. Ge, F. Lisdat, and F. W. Scheller, "Electrochemistry of Cytochrome c Immobilized on Colloidal Gold Modified Carbon Paste Electrodes and Its Electrocatalytic Activity," *Electroanalysis,* vol. 14, no. 2, pp. 141-147, 2002/01/01, 2002.
[27] D. C. Prabhakaran, J. Riotte, Y. Sivry, and S. Subramanian, "Electroanalytical Detection of Cr(VI) and Cr(III) Ions Using a Novel Microbial Sensor,"

doi:10.6342/NTU202401040

Electroanalysis, vol. 29, no. 5, pp. 1222-1231, 2017/05/01, 2017.
[28] D. P. Jaihindh, B. Thirumalraj, S.-M. Chen, P. Balasubramanian, and Y.-P. Fu, "Facile synthesis of hierarchically nanostructured bismuth vanadate: An efficient photocatalyst for degradation and detection of hexavalent chromium," *Journal of Hazardous Materials,* vol. 367, pp. 647-657, 2019/04/05/, 2019.
[29] K. Molaei, H. Bagheri, A. A. Asgharinezhad, H. Ebrahimzadeh, and M. Shamsipur, "SiO2-coated magnetic graphene oxide modified with polypyrrole–polythiophene: A novel and efficient nanocomposite for solid phase extraction of trace amounts of heavy metals," *Talanta,* vol. 167, pp. 607-616, 2017/05/15/, 2017.
[30] E. Kazemi, A. M. Haji Shabani, S. Dadfarnia, and F. Izadi, "Speciation and determination of chromium ions by dispersive micro solid phase extraction using magnetic graphene oxide followed by flame atomic absorption spectrometry," *International Journal of Environmental Analytical Chemistry,* vol. 97, no. 11, pp. 1080-1093, 2017/09/02, 2017.
[31] K. Dashtian, M. Ghaedi, and S. Hajati, "Photo-Sensitive Pb5S2I6 crystal incorporated polydopamine biointerface coated on nanoporous TiO2 as an efficient signal-on photoelectrochemical bioassay for ultrasensitive detection of Cr(VI) ions," *Biosensors and Bioelectronics,* vol. 132, pp. 105-114, 2019/05/01/, 2019.
[32] A. Yari, and H. Bagheri, "Determination of Cr(VI) with Selective Sensing of Cr(VI) Anions by a PVC-Membrane Electrode Based on Quinaldine Red," *Journal of the Chinese Chemical Society,* vol. 56, no. 2, pp. 289-295, 2009/04/01, 2009.
[33] S. Shahim, R. Sukesan, I. Sarangadharan, and Y. L. Wang, "Multiplexed Ultra-Sensitive Detection of Cr(III) and Cr(VI) Ion by FET Sensor Array in a Liquid Medium," *Sensors (Basel),* vol. 19, no. 9, Apr 26, 2019.
[34] B. Liu, Y. Lei, and B. Li, "A batch-mode cube microbial fuel cell based "shock" biosensor for wastewater quality monitoring," *Biosensors and Bioelectronics,* vol. 62, pp. 308-314, 2014/12/15/, 2014.
[35] H. Chung, W. J. Ju, E. H. Jho, and K. Nam, "Applicability of a submersible microbial fuel cell for Cr(VI) detection in water," *Environmental Monitoring and Assessment,* vol. 188, no. 11, pp. 613, 2016/10/12, 2016.
[36] E. O. Jorge, M. M. Rocha, I. T. E. Fonseca, and M. M. M. Neto, "Studies on the stripping voltammetric determination and speciation of chromium at a rotating-disc bismuth film electrode," *Talanta,* vol. 81, no. 1, pp. 556-564, 2010/04/15/, 2010.
[37] M. Grabarczyk, "Speciation Analysis of Chromium by Adsorptive Stripping Voltammetry in Tap and River Water Samples," *Electroanalysis,* vol. 20, no. 20, pp. 2217-2222, 2008/10/01, 2008.
[38] C. Wang, and C. K. Chan, "Carbon Nanotube–Based Electrodes for Detection of Low–ppb Level Hexavalent Chromium Using Amperometry," *ECS Journal of Solid State Science and Technology,* vol. 5, no. 8, pp. M3026, 2016/03/08, 2016.
[39] Z. Stojanović, Z. Koudelkova, E. Sedlackova, D. Hynek, L. Richtera, and V. Adam, "Determination of chromium(vi) by anodic stripping voltammetry using a silver-plated glassy carbon electrode," *Analytical Methods,* vol. 10, no. 24, pp. 2917-2923, 2018.
[40] A. García-Miranda Ferrari, P. Carrington, S. J. Rowley-Neale, and C. E. Banks, "Recent advances in portable heavy metal electrochemical sensing platforms," *Environmental Science: Water Research & Technology,* vol. 6, no. 10, pp. 2676-

doi:10.6342/NTU202401040

2690, 2020.
[41] S. Hassan, M. S. El-Shahawi, A. Othman, and M. Mosaad, “A Potentiometric Rhodamine-B Based Membrane Sensor for the Selective Determination of Chromium Ions in Wastewater,” *Analytical Sciences,* vol. 21, pp. 673-678, 07/01, 2005.
[42] P. Bergveld, “Thirty years of ISFETOLOGY: What happened in the past 30 years and what may happen in the next 30 years,” *Sensors and Actuators B: Chemical,* vol. 88, no. 1, pp. 1-20, 2003/01/01/, 2003.
[43] M. Baylav, *Ion-sensitive field effect transistor (ISFET) for MEMS multisensory chips at RIT*: Rochester Institute of Technology, 2010.
[44] 阎秉峰, “离子选择性电极的工作原理,” *内蒙古科技与经济,* vol. 3, pp. 106-109, 2005.
[45] R. Sharma, M. Geranpayehvaghei, F. Ejeian, A. Razmjou, and M. Asadnia, “Recent advances in polymeric nanostructured ion selective membranes for biomedical applications,” *Talanta,* vol. 235, pp. 122815, 2021/12/01/, 2021.
[46] C. Tang, and M. L. Bruening, “Ion separations with membranes,” *Journal of Polymer Science,* vol. 58, no. 20, pp. 2831-2856, 2020/10/15, 2020.
[47] V. M. Keresten, A. G. Bykov, I. V. Gofman, E. V. Solovyeva, A. Y. Vlasov, and K. N. Mikhelson, “Non-constancy of the bulk resistance of ionophore-based ion-selective membranes within the Nernstian response range: A semi-quantitative explanation,” *Journal of Membrane Science,* vol. 683, pp. 121830, 2023/10/05/, 2023.
[48] M. Waleed Shinwari, M. Jamal Deen, and D. Landheer, “Study of the electrolyte-insulator-semiconductor field-effect transistor (EISFET) with applications in biosensor design,” *Microelectronics Reliability,* vol. 47, no. 12, pp. 2025-2057, 2007/12/01/, 2007.
[49] Y. J. Huang, C. C. Lin, J. C. Huang, C. H. Hsieh, C. H. Wen, T. T. Chen, L. S. Jeng, C. K. Yang, J. H. Yang, F. Tsui, Y. S. Liu, S. Liu, and M. Chen, "High performance dual-gate ISFET with non-ideal effect reduction schemes in a SOI-CMOS bioelectrical SoC." pp. 29.2.1-29.2.4.
[50] P. D. v. d. Wal, D. Briand, G. Mondin, S. Jenny, S. Jeanneret, C. Millon, H. Roussel, C. Dubourdieu, and N. F. d. Rooij, "High-k dielectrics for use as ISFET gate oxides." pp. 677-680 vol.2.
[51] C. Xiao-Wen, and H. Nien-Tsu, “Multi-ion Selective Membrane Deposited Dual-gate Ion-Sensitive Field-Effect Transistor (DG-ISFET) Integrating the Microchamber Embedded Trench and Filter Membrane for Whole Blood Preparation and Ions Concentration Test in Blood,” Graduate Institute of Biomedical Electronics and Bioinformatics, National Taiwan University, Taipei, 2022.
[52] S. Jia, G. Li, P. Liu, R. Cai, H. Tang, B. Xu, Z. Wang, Z. Wu, K. Wang, and X. W. Sun, “Highly Luminescent and Stable Green Quasi-2D Perovskite-Embedded Polymer Sheets by Inkjet Printing,” *Advanced Functional Materials,* vol. 30, no. 24, pp. 1910817, 2020.
[53] Y. Fang, K. Yang, Y. Zhang, C. Peng, A. Robledo-Cabrera, and A. López-Valdivieso, “Highly surface activated carbon to remove Cr(VI) from aqueous solution with adsorbent recycling,” *Environmental Research,* vol. 197, pp. 111151, 2021/06/01/, 2021.

doi:10.6342/NTU202401040